hep-ph/0108191
23 August 2001

Bayesian View Of Solar Neutrino Oscillations

M.V. Garzelli and C. Giunti
INFN, Sezione di Torino,
and
Dipartimento di Fisica Teorica, Università di Torino,
Via P. Giuria 1, I–10125 Torino, Italy

Abstract

We present the results of a Bayesian analysis of solar neutrino data in terms of $\nu_e \to \nu_{\mu,\tau}$ and $\nu_e \to \nu_s$ oscillations, where ν_s is a sterile neutrino. We perform a Rates Analysis of the rates of solar neutrino experiments, including the first SNO CC result, and spectral data of the CHOOZ experiment, and a Global Analysis that takes into account also the Super-Kamiokande day and night electron energy spectra. We show that the Bayesian analysis of solar neutrino data does not suffer any problem from the inclusion of the numerous bins of the CHOOZ and Super-Kamiokande electron energy spectra and allows to reach the same conclusions on the favored type of neutrino transitions and on the determination of the most favored values of the oscillation parameters in both the Rates and Global Analysis. Our Bayesian analysis shows that $\nu_e \to \nu_s$ transitions are strongly disfavored with respect to $\nu_e \to \nu_{\mu,\tau}$ transitions. In the case of $\nu_e \to \nu_{\mu,\tau}$ oscillations, the Large Mixing Angle region is favored by the data (85% probability), the LOW region has some small chance (13% probability), the Vacuum Oscillation region is almost excluded (2% probability) and the Small Mixing Angle region is practically excluded (0.01% probability). We calculate also the marginal posterior probability distributions for $\tan^2\vartheta$ and Δm^2 in the case of $\nu_e \to \nu_{\mu,\tau}$ oscillations and we show that the data imply large mixing almost with certainty and large values of Δm^2 are favored ($2 \times 10^{-6}\,\mathrm{eV}^2 < \Delta m^2 < 10^{-3}\,\mathrm{eV}^2$ with 85% probability). We present also the results of a standard least-squares analysis of solar neutrino data and we show that the standard goodness of fit test is not able to rejects pure $\nu_e \to \nu_s$ transitions. The likelihood ratio test allows to reject pure $\nu_e \to \nu_s$ transitions in favor of $\nu_e \to \nu_{\mu,\tau}$ transitions only in the Global Analysis.

1 Introduction

The experimental investigation of the solar neutrino problem (see [1]) has received recently a fundamental contribution from the first data of the SNO solar neutrino experiment [2], in which charged-current interactions of solar ^{8}B electron neutrinos with deuterium have been observed with a rate about 0.35 times of that predicted by the BP2000 Standard Solar Model (SSM) [3]. A model independent comparison of SNO and Super-Kamiokande [4] data show that ν_μ or ν_τ are present in the flux of solar neutrino on Earth at 3.06σ [2, 5] (see Ref. [6] for a discussion on the probability content of this statement). Since the simplest explanation of the presence of ν_μ or ν_τ in the flux of solar neutrino on Earth is neutrino oscillations due to neutrino masses and mixing (see [7]), this is the second model-independent evidence in favor of neutrino mixing, after the up-down asymmetry of multi-GeV atmospheric ν_μ-induced events discovered in the Super-Kamiokande experiment [8].

In the simplest case of mixing of two neutrinos ν_e and ν_x that we consider here, we have

$$\begin{aligned} \nu_e &= \cos\vartheta\,\nu_1 + \sin\vartheta\,\nu_2\,, \\ \nu_x &= -\sin\vartheta\,\nu_1 + \cos\vartheta\,\nu_2\,, \end{aligned} \tag{1}$$

where ϑ is the mixing angle and ν_1, ν_2 are massive neutrinos with masses m_1, m_2, respectively. The flavor neutrino ν_x could be either active, $x = a$ with $a = \mu, \tau$, or sterile, $x = s$ (see [7]).

Following the release of the SNO first results, the data of solar neutrino experiments (Homestake [9], GALLEX [10], SAGE [11], GNO [12], Super-Kamiokande [4], SNO [2]) have been analyzed in terms of neutrino oscillations in Refs. [5, 13, 14, 15]. The above-mentioned 3.06σ model-independent evidence in favor of the presence of ν_μ or ν_τ in the flux of solar neutrino on Earth clearly implies that the solution of the solar neutrino problem in terms of oscillations of solar ν_e's into active ν_μ or ν_τ is strongly favored with respect to transitions into sterile neutrinos ν_s (see also [16]). Therefore, assuming the BP2000 SSM prediction for the neutrino fluxes produced in the core of the Sun [3] and using a standard least-squares analysis, the authors of Refs. [5, 14] calculated only the allowed regions in the plane of the oscillation parameters $\tan^2\vartheta$ and Δm^2 in the case of $\nu_e \to \nu_a$ transitions ($\Delta m^2 \equiv m_2^2 - m_1^2$)[1].

The standard least-squares method for the analysis of solar neutrino data is an approximation of the rigorous frequentist method to calculate allowed regions with exact coverage [21, 22, 23]. It has been shown in Refs. [21, 23] that an analysis of solar neutrino data with a rigorous frequentist method may lead results that differ significantly from those obtained with the standard least-squares method. Unfortunately the implementation of a rigorous frequentist method in the analysis of solar neutrino data is complicated and computer-time consuming because it is necessary to calculate the distribution probability of the estimator of the parameters for all possible values of the parameters. Moreover, several rigorous frequentist methods are available and it is not clear which is the most appropriate (if there is one) for the analysis of solar neutrino data (see Refs. [21, 22, 23] and references therein).

[1] The authors of Ref. [13] took into account the very interesting possibility of simultaneous $\nu_e \to \nu_a$ and $\nu_e \to \nu_s$ transitions, that is allowed in four-neutrino mixing schemes (see [7, 17, 18, 19, 20] and references therein). In this case, besides $\tan^2\vartheta$ and Δm^2, there is an additional parameter $\cos^2\eta$ that regulates the relative amount of $\nu_e \to \nu_a$ and $\nu_e \to \nu_s$ transitions ($0 \leq \eta \leq \pi/2$). We do not consider here this possibility because of its computational difficulties (in the Bayesian analysis it is necessary to integrate the posterior probability distribution function for the oscillation parameters over $\cos^2\eta$).

In this paper we present the results of an analysis of solar neutrino data in terms of two-neutrino oscillations in the framework of Bayesian Probability Theory. This analysis has practically the same difficulties of the standard least-squares analysis and can therefore be easily performed by the groups specialized in the analysis of solar neutrino data.

The Bayesian analysis of solar neutrino data is not approximate as the least-squares analysis in the framework of Frequentist Statistics. Furthermore, Bayesian Probability Theory has several advantages over Frequentist Statistics, that have been discussed in several books and papers (see [24, 25, 26, 27, 28]). Here we notice only a few facts:

1. All human statements, including scientific ones, represent knowledge (belief) with some degree of uncertainty. Bayesian Probability Theory allows to quantify this uncertainty through the natural definition of probability as degree of belief.

2. Bayesian Probability Theory allows to calculate through Bayes Theorem the improvement of knowledge as a consequence of experimental measurements. This is how our mind works and how science improves. Therefore, Bayesian Probability Theory is the natural statistical tool for scientists.

3. Probability of an event in Frequentist Statistics is defined as the asymptotic relative frequency of occurrence of the event in an infinite set of experiments. Obviously such set is never available in practice. Therefore, Frequentist Statistics is based on imaginary data. On the other hand, all inferences in Bayesian Probability Theory are based only on the data that actually occurred.

4. Because of the definition of probability in Frequentist Statistics, the results obtained have usually good properties (*i.e.* they are reliable) only in the case of large data sets. In frontier research often a small number of experimental data are available (as in the case of solar neutrinos) and the scientist is not interested in long-term behavior of inferences, but in getting the best possible inference from the available data. Bayesian Probability Theory satisfies this wish.

5. Results in Frequentist Statistics are based on hypothetical data, *i.e.* data that could have been observed but did not occur. Often different scientists may have different ideas on which are the relevant hypothetical data, leading to different conclusions (for example, the so-called "optional stopping problem" is well known and discussed in the literature).

6. In Frequentist Statistics there is no way to take into account theoretical and systematical errors, that are not random variables. Nevertheless, since the great majority of scientific measurements suffer of systematic errors and scientific inferences depend on theoretical errors (they are both crucial in the analysis of solar neutrino data), frequentists treat these errors as if they were random variables. Nobody knows the meaning of results obtained in this way, with an inconsistent method. Bayesian Probability Theory obviously can treat theoretical and systematical errors on the same footing as statistical ones, leading to consistent results.

7. Once a problem is well posed the application of Bayesian Probability Theory is clear and straightforward and leads to unique results. On the other hand, in the framework of Frequentist Statistics several arbitrary and difficult choices that can lead to different results are necessary. That is why popular methods (as least-squares) that sometimes have poor performances are widely used without a real understanding of the motivations.

8. Since Bayesian Probability Theory allows to calculate the improvement of knowledge as a consequence of physical observations, a prior knowledge is necessary. It has been argued by advocates of Frequentist Statistics that prior knowledge is subjective, leading to undesirable subjectivity in the derivation of scientific results (forgetting the often less clear subjective choices of method, estimator, etc. necessary in Frequentist Statistics). On this problem widely discussed in the literature we want only to remark that all human activities, including scientific research, have some degree of subjectivity, but communication and collaboration among people working in a field allow to reach an agreement on the most reasonable prior knowledge in the field and a way to quantify it. Once the prior knowledge is fixed, Bayesian Probability Theory leads to unique conclusions.

The plan of the paper is as follows. In Section 2 we perform a standard least-squares analysis of solar neutrino data. From the calculational point of view this is not an additional task, because the calculation of the least-squares function is a necessary step in order to derive the Bayesian probability distribution for the parameters. We consider the two cases of $\nu_e \to \nu_a$ transitions (Active)[2], and $\nu_e \to \nu_s$ transitions (Sterile). In Section 3 we present our Bayesian analysis of solar neutrino data. In Section 3.1 we compare the probabilities of the models with $\nu_e \to \nu_a$ and $\nu_e \to \nu_s$ transitions. In Section 3.2 we present the results of our calculation of Bayesian allowed regions (credible regions) in the $\tan^2\vartheta$–Δm^2 plane for Active transitions. In Section 3.3 we marginalize the posterior Bayesian probability distribution for Active transitions in order to calculate the posterior Bayesian probability distributions for $\tan^2\vartheta$ and Δm^2. Finally, in Section 4 we draw our conclusions.

In both the standard least-squares and Bayesian analyses we consider first only the total rates measured by solar neutrino experiments (Rates Analysis) and then the total rates of the Homestake, GALLEX+GNO+SAGE, SNO experiments and the Super-Kamiokande day and night electron energy spectra (Global Analysis). In both the Rates Analysis and the Global Analysis we consider also the data of the CHOOZ experiment, that are important because they exclude large values of the mixing angle for $\Delta m^2 \gtrsim 10^{-3}\,\mathrm{eV}^2$ [31]. Therefore, we consider only values of Δm^2 smaller than $10^{-3}\,\mathrm{eV}^2$ and we will see that, consistently, the allowed regions for the oscillation parameters are limited below this value of Δm^2.

In this paper we use the standard names for the regions in $\tan^2\vartheta$–Δm^2 plane (see [7]):

[2]The treatment of solar $\nu_e \to \nu_a$ transitions in the framework of the simple two-neutrino mixing scheme in Eq. (1) with $\nu_x = \nu_a$ is valid with good approximation in the case of mixing of three neutrinos (ν_e, ν_μ, ν_τ) with small U_{e3} [29, 30], as indicated by the results of the CHOOZ long-baseline $\bar{\nu}_e$ disappearance experiment [31]. In this case ν_a is a linear combination of ν_μ and ν_τ. Furthermore, the treatment is also valid in 3+1 four-neutrino mixing schemes in which the sterile neutrino is practically decoupled from the active ones ($1 - |U_{s4}|^2 \ll 1$) [32] and U_{e3} is small, as indicated by CHOOZ data [19].

Small Mixing Angle (SMA) for

$$10^{-4} < \tan^2\vartheta < 10^{-1}\,, \quad 10^{-8}\,\mathrm{eV}^2 < \Delta m^2 < 10^{-3}\,\mathrm{eV}^2\,, \tag{2}$$

Large Mixing Angle (LMA) for

$$10^{-1} < \tan^2\vartheta < 10\,, \quad 2\times 10^{-6}\,\mathrm{eV}^2 < \Delta m^2 < 10^{-3}\,\mathrm{eV}^2\,, \tag{3}$$

LOW for

$$10^{-1} < \tan^2\vartheta < 10\,, \quad 10^{-8}\,\mathrm{eV}^2 < \Delta m^2 < 2\times 10^{-6}\,\mathrm{eV}^2\,, \tag{4}$$

Vacuum Oscillation (VO) for

$$10^{-1} < \tan^2\vartheta < 10\,, \quad 10^{-11}\,\mathrm{eV}^2 < \Delta m^2 < 10^{-8}\,\mathrm{eV}^2\,. \tag{5}$$

2 Standard Least-Squares Analysis

In our standard least-squares analysis (often called "χ^2 analysis") we consider first in the Rates Analysis of Section 2.1 only the total rates measured by solar neutrino experiments (see Table 1), and the CHOOZ positron spectra given in Ref. [31]. Then in the Global Analysis of Section 2.2 we consider also the Super-Kamiokande data on the day and night electron energy spectra.

2.1 Rates Analysis

Our least-squares function for the Rates Analysis is written as

$$X^2 = X^2_{\mathrm{S}} + X^2_{\mathrm{C}}\,, \tag{6}$$

where X^2_{S} takes into account the rates measured in solar neutrino experiments and X^2_{C} takes into account the data of the CHOOZ experiment.

The X^2 of the solar neutrino rates, X^2_{S}, is calculated using the procedure described in Refs. [33, 30, 34, 21]:

$$X^2_{\mathrm{S}} = \sum_{j_1,j_2=1}^{N_{\mathrm{S}}} \left(R^{(\mathrm{ex})}_{j_1} - R^{(\mathrm{th})}_{j_1}\right) (V^{-1}_{\mathrm{S}})_{j_1 j_2} \left(R^{(\mathrm{ex})}_{j_2} - R^{(\mathrm{th})}_{j_2}\right)\,, \tag{7}$$

where V_{S} is the covariance matrix of experimental and theoretical uncertainties, $R^{(\mathrm{ex})}_j$ is the event rate measured in the j^{th} experiment and $R^{(\mathrm{th})}_j$ is the corresponding theoretical event rate, that depends on Δm^2 and $\tan^2\theta$. The indices $j, j_1, j_2 = 1, \ldots, N_{\mathrm{S}}$ with $N_{\mathrm{S}} = 4$ indicate the four types of solar neutrino experiments listed in order in Table 1 together with the corresponding event rates and experimental uncertainties.

The covariance matrix $V_{\rm S}$ takes into account the experimental and theoretical uncertainties added in quadrature[3] [33, 30, 34, 21]:

$$(V_{\rm S})_{j_1,j_2} = \delta_{j_1,j_2}\sigma_{j_1}^2 + \delta_{j_1,j_2}\left(\sum_{i_1=1}^{8} R_{i_1,j_1}^{(\rm th)}\Delta\ln C_{i_1,j_1}^{(\rm th)}\right)^2 + \sum_{i_1,i_2=1}^{8} R_{i_1,j_1}^{(\rm th)} R_{i_2,j_2}^{(\rm th)} \sum_{k=1}^{12}\alpha_{i_1,k}\alpha_{i_2,k}\left(\Delta\ln X_k\right)^2 , \tag{8}$$

where σ_j^2 are the experimental uncertainties given in Table 1, calculated by adding in quadrature the statistical and systematic uncertainty for each experiment[4]. The indices $i, i_1, i_2 = 1, \ldots, 8$ denote the solar neutrino fluxes produced in the eight solar thermonuclear reactions *pp*, *pep*, *hep*, Be, B, N, O, F, respectively. The index $k = 1, \ldots, 12$ labels the twelve input astrophysical parameters X_k in the SSM ($S_{1,1}$, $S_{3,3}$, $S_{3,4}$, $S_{1,14}$, $S_{1,7}$, Luminosity, Z/X, Age, Opacity, Diffusion, $C_{\rm Be}$, $S_{1,16}$), whose relative uncertainties $\Delta\ln X_k$ determine the correlated uncertainties of the neutrino fluxes $\Phi_i^{\rm SSM}$ through the logarithmic derivatives

$$\alpha_{i,k} = \frac{\partial \ln\Phi_i^{\rm SSM}}{\partial \ln X_k} . \tag{9}$$

We adopt the values of $\alpha_{i,k}$ and $\Delta\ln X_k$ given in Ref. [30], except for $\Delta\ln X_7$ (relative to Z/X), whose value has been updated in the BP2000 SSM [3] from 0.033 to 0.061, and $\alpha_{i,12} = \delta_{i,8}$, $\Delta\ln X_{12} = 0.181$, that have been introduced for the first time in the BP2000 SSM [3]. X_{12} is the S-factor for the reaction $^{16}{\rm O}(p,\gamma)^{17}{\rm F}$ that determines the small F neutrino flux ($i = 8$). With these values we calculate the fractional uncertainties of the SSM neutrino fluxes

$$\Delta\ln\Phi_i^{\rm SSM} = \sqrt{\sum_{k=1}^{12}\left(\alpha_{i,k}\,\Delta\ln X_k\right)^2} \tag{10}$$

listed in Table 2. One can see that these fractional uncertainties are in good agreement with those presented in Table 7 of Ref. [3]. The uncertainty of the *hep* flux is rather small, in view of the fact that no uncertainty is given in Ref. [3] because of the difficulty in calculating the S-factor of the *hep* reaction. However, this is irrelevant for our calculation because in any case the contribution of the *hep* flux to solar neutrino data is negligible (the Super-Kamiokande collaboration [4] found that the flux of *hep* neutrinos on Earth is less than 4.3 times the BP2000 SSM prediction at 90% CL, that is one hundred times smaller than the B neutrino flux).

The quantity

$$R_{i,j}^{(\rm th)} = \Phi_i^{\rm SSM}\; C_{i,j}^{(\rm th)}\; P_{i,j}^{(\rm th)}(\Delta m^2, \tan^2\theta) , \tag{11}$$

such that

$$R_j^{(\rm th)} = \sum_{i=1}^{8} R_{i,j}^{(\rm th)} , \tag{12}$$

[3] This is the common practice, in spite of the impossibility to treat theoretical uncertainties in the framework of Frequentist Statistics (see item 6 in Section 1).

[4] Also this common practice is completely unjustified in the framework of Frequentist Statistics (see item 6 in Section 1).

is the theoretical event rate in the $j^{\rm th}$ experiment due to the neutrino flux $\Phi_i^{\rm SSM}$ produced in the $i^{\rm th}$ thermonuclear reaction in the sun according to the BP2000 Standard Solar Model [3]. $C_{i,j}^{\rm (th)}$ is the corresponding energy-averaged cross section and $P_{i,j}^{\rm (th)}(\Delta m^2, \tan^2\theta)$ is the corresponding averaged survival probability of solar ν_e's, that depends on Δm^2 and $\tan^2\theta$ (in the case of the Super-Kamiokande experiment, $j = 4$, also the averaged $\nu_e \to \nu_a$ transition probability must be properly taken into account). The quantity $\Delta \ln C_{i,j}^{\rm (th)} = \Delta C_{i,j}^{\rm (th)} / C_{i,j}^{\rm (th)}$ is the relative uncertainty of the energy-averaged cross section $C_{i,j}^{\rm (th)}$. The values of $\Delta \ln C_{i,j}^{\rm (th)}$ for $j = 1, 2, 4$ (^{37}Cl, ^{71}Ga and H_2O experiments) are given in Ref. [30]. For the SNO experiment ($j = 3$) $\Delta \ln C_{3,3}^{\rm (th)} = \Delta \ln C_{5,3}^{\rm (th)} = 3.0 \times 10^{-2}$ and the others are zero.

For the calculation of the probabilities $P_{i,j}^{\rm (th)}(\Delta m^2, \tan^2\theta)$ we have used the tables of neutrino spectra, solar density and radiochemical detector cross sections available in Bahcall's web pages [35], BP2000 Standard Solar Model [3]. For the calculation of the theoretical rate of the SNO experiment we used the charged-current cross section given in Refs. [36, 37]. The probability of neutrino oscillations is calculated with an unified approach that allows to pass continuously from the vacuum oscillation regime to MSW transitions [38] through the quasi-vacuum regime [39, 40], using the quasi-vacuum analytical prescription given in Ref. [41], the usual prescription for the MSW survival probability (see [40, 42]) and the level crossing probability appropriate for an exponential density profile [43, 44]. We calculate the regeneration in the Earth using a two-step model of the Earth density profile [45, 46, 47, 48, 49], that is known to produce results that do not differ appreciably from those obtained with a less approximate density profile.

The X^2 of the CHOOZ positron spectra, $X^2_{\rm C}$ is calculated as in the analysis A of Ref. [31], with the following approximations. Since we do not know the antineutrino spectrum, the spatial distribution functions of the reactor cores and detector and the detector response function linking the real and visible positron energies, for each energy bin we calculated the oscillation probability at the average energy of the bin and the average distance of the detector from each of the two reactors [50]. This approximation is quite good because we are interested in values of Δm^2 below $10^{-3}\,$eV, for which the energy and distance dependence of the survival probability of the $\bar\nu_e$'s in the CHOOZ experiment is very weak. We calculate $X^2_{\rm C}$ as in Eq. (13) of Ref. [31], with the only difference that we neglect the energy-scale calibration factor, whose small uncertainty (1.1%) is practically negligible:

$$X^2_{\rm C} = \sum_{j_1,j_2=1}^{N_{\rm C}} \left(R_{j_1}^{\rm (th)} - \alpha_{\rm C}\, R_{j_1}^{\rm (ex)} \right) (V_{\rm C}^{-1})_{j_1 j_2} \left(R_{j_2}^{\rm (th)} - \alpha_{\rm C}\, R_{j_2}^{\rm (ex)} \right) + \left(\frac{\alpha_{\rm C} - 1}{\sigma_{\alpha_{\rm C}}} \right)^2 , \qquad (13)$$

where $N_{\rm C} = 14$ is the number of energy bins and $\alpha_{\rm C}$ is the absolute normalization constant with uncertainty $\sigma_{\alpha_{\rm C}} = 2.7 \times 10^{-2}$ [31]. We calculate the CHOOZ covariance matrix $V_{\rm C}$ as described in Eq. (12) of Ref. [31]. The only missing information in Ref. [31] is the value of the systematic uncertainties of the positron energy bins, for which only the values for positron energy 2 and 6 MeV are given. For the other bins we take systematic uncertainties interpolated linearly between these two values.

The values of the minimum $X^2_{\rm min}$ of the least-squares function (6) and the corresponding best-fit values of the oscillation parameters for $\nu_e \to \nu_a$ or $\nu_e \to \nu_s$ transitions are given in the first two rows of Table 3. The contribution to $X^2_{\rm min}$ from the CHOOZ least-squares function

$X^2_{\rm C}$ is always 6.0, in reasonable agreement with the minimum value $(X^2_{\rm min})_{\rm CHOOZ} = 5.0$ and $(X^2_{\rm no-oscillations})_{\rm CHOOZ} = 5.5$ found by the CHOOZ collaboration in Ref. [31].

One can see from Table 3 that the minimum $X^2_{\rm min}$ lies in the Vacuum Oscillation (VO) region for both Active and Sterile transitions. Therefore, there are two minima corresponding to the same value of $\sin^2 2\vartheta$ (they are connected by $\log\tan^2\vartheta \to -\log\tan^2\vartheta$).

As written in Table 3, the number of degrees of freedom (n.d.f.) in the Rates Analysis is 15, given by 4 solar rates plus 14 CHOOZ bins minus 3 parameters ($\alpha_{\rm C}$, $\tan^2\vartheta$, Δm^2). The goodness of fit obtained assuming for $X^2_{\rm min}$ a χ^2 distribution with n.d.f. degrees of freedom (see Refs. [21, 23] for a discussion on the approximate character of this assumption) is more than acceptable for both Active and Sterile transitions.

In Table 3 we report the goodness of fit as usual in the standard least-squares analysis of solar neutrino data. However, let us remark that its significance is quite doubtful. Indeed, by definition the goodness of fit is the probability to observe a worse value for $X^2_{\rm min}$ assuming that the true values of the parameters are those corresponding to the measured $X^2_{\rm min}$. It is not clear what is the relevance of this probability to observe values of $X^2_{\rm min}$ that have not been observed. Therefore, we think that the exact value of the goodness of fit has no meaning. Only its order of magnitude may be useful to give an indication of the quality of the fit.

However, the large value of the goodness of fit in the first two rows in Table 3 looks suspicious: if the assumption of a χ^2 distribution with n.d.f. degrees of freedom for $X^2_{\rm min}$ is approximately correct, the expected value of $X^2_{\rm min}$ is equal to n.d.f. = 15, which would give a goodness of fit of about 45%. The small value of $X^2_{\rm min}$ is mainly due to the inclusion in the fit of the 14 energy bins of the CHOOZ experiment, that contribute with 13 degrees of freedom and give a contribution of only 6.0 to $X^2_{\rm min}$. This problem is already present in the analysis of CHOOZ data performed by the CHOOZ collaboration [31], where a value of $(X^2_{\rm min})_{\rm CHOOZ} = 5.0$ was found with 11 degrees of freedom.

From the second row in Table 3 and taking into account that the fit of the four solar neutrino rates contributes with 5.3 to the value of $X^2_{\rm min}$, one could conclude that the explanation of the solar neutrino problem in terms of $\nu_e \to \nu_s$ transitions is acceptable. This conclusion would be in contradiction with the model-independent evidence in favor of the presence of active $\nu_{\mu,\tau}$ in the flux of solar neutrinos on Earth discussed in Refs. [2, 5, 6]. This apparent contradiction is resolved by noting that the model-independent calculations performed in Refs. [2, 5, 6] are based on the adjustment of the Super-Kamiokande electron energy threshold in order to make the response functions of the SNO and Super-Kamiokande experiments to solar neutrinos approximately equal [51, 52]. The authors of Ref. [5] found that, given the SNO threshold $T_e^{\rm SNO} = 6.75\,{\rm MeV}$, the SNO and Super-Kamiokande response functions are approximately equal for the Super-Kamiokande threshold $T_e^{\rm SK} = 8.6\,{\rm MeV}$, instead of $T_e^{\rm SK} = 4.5\,{\rm MeV}$ for which the rate in the fourth row of Table 1 has been obtained [4]. The low $X^2_{\rm min}$ that we find in the VO region is due to the strong energy dependence of the $\nu_e \to \nu_s$ transition probability in the case of vacuum oscillations, such that the averaged transition probability is quite different in the SNO and Super-Kamiokande experiments if their response function are different. Indeed, for the values of $\tan^2\vartheta$ and Δm^2 corresponding to $X^2_{\rm min}$ we have $\langle P_{\nu_e\to\nu_e}\rangle_{\rm SNO} = 0.347$ and $\langle P_{\nu_e\to\nu_e}\rangle_{\rm SK} = 0.504$.

We have repeated our least-squares analysis using $T_e^{\rm SK} = 8.6\,{\rm MeV}$ and the corresponding

rate 0.451 ± 0.017 [4, 5] for the Super-Kamiokande experiment, normalized to the BP2000 SSM prediction, and we found $X^2_{\rm min} = 14.7$ for $\tan^2\vartheta = 1.4\times10^{-3}$ and $\Delta m^2 = 6.0\times10^{-6}\,{\rm eV}^2$, *i.e.* in the SMA region. Now the contribution to $X^2_{\rm min}$ from the fit of the four solar neutrino rates is 8.7, in reasonable agreement with the model-independent 3.06σ exclusion of pure $\nu_e \to \nu_s$ transitions discussed in Refs. [2, 5, 6], which would imply a contribution of about 9.4 to $X^2_{\rm min}$. The discrepancy is due to the small remaining difference of the SNO and Super-Kamiokande response functions (see Fig. 1 of Ref. [5]), such that the averaged $\nu_e \to \nu_s$ transition probabilities in the SNO and Super-Kamiokande experiments are not exactly equal: for the values of $\tan^2\vartheta$ and Δm^2 corresponding to $X^2_{\rm min}$ we have $\langle P_{\nu_e\to\nu_e}\rangle_{\rm SNO} = 0.453$ and $\langle P_{\nu_e\to\nu_e}\rangle_{\rm SK} = 0.459$. Indeed, using "by hand" the same averaged probabilities of $\nu_e \to \nu_s$ transitions for the SNO and Super-Kamiokande experiments, we obtain $X^2_{\rm min} = 15.5$, corresponding to a contribution of 9.5 from the fit of the four solar neutrino rates.

Even using "by hand" the same averaged probabilities of $\nu_e \to \nu_s$ transitions for the SNO and Super-Kamiokande experiments, the goodness of fit is high, 42%. Therefore, we see that in the present situation the goodness of fit is practically useless, because it cannot exclude in any way pure $\nu_e \to \nu_s$ transitions that are excluded at 3.06σ with a model-independent analysis of the data [2, 5, 6]. Actually, from Table 3 one could naively think that $\nu_e \to \nu_s$ transitions are favored over $\nu_e \to \nu_a$ transitions because the value of $X^2_{\rm min}$ is closer to the expected value given by the number of degrees of freedom. This is a clear example of the failures and paradoxes that sometimes are encountered in the framework of Frequentist Statistics.

However, the goodness of fit test is considered to be appropriate for testing an hypothesis against all possible alternatives (see [53]). A better test for alternative hypotheses is the likelihood ratio test[5], for which we find

$$\frac{{\rm Max}_{\tan^2\vartheta,\Delta m^2,\alpha_{\rm C}}\, p^{\rm (S)}({\rm D}|\tan^2\vartheta,\Delta m^2,\alpha_{\rm C})}{{\rm Max}_{\tan^2\vartheta,\Delta m^2,\alpha_{\rm C}}\, p^{\rm (A)}({\rm D}|\tan^2\vartheta,\Delta m^2,\alpha_{\rm C})} = 0.24\,, \tag{14}$$

with the probability distribution functions

$$p^{\rm (T)}({\rm D}|\tan^2\vartheta,\Delta m^2,\alpha_{\rm C}) = \frac{e^{-X^2_{\rm S}/2}}{(2\pi)^{N_{\rm S}/2}\sqrt{|V_{\rm S}|}}\,\frac{e^{-X^2_{\rm C}/2}}{(2\pi)^{N_{\rm C}/2}\sqrt{|V_{\rm C}|}}\,, \tag{15}$$

where D represents the data, and T = A for $\nu_e \to \nu_a$ transitions (Active) and T = S for $\nu_e \to \nu_s$ transitions (Sterile).

In Eq. (14) we have considered Sterile transitions as the null hypothesis and Active transitions as the alternative hypothesis, in order to see if the null hypothesis should be rejected or not. This choice is one of the arbitrary choices necessary in the application of

[5]We note, in passing, that in the case of Active transitions the maximum likelihood is reached in the LMA region for $\tan^2\vartheta = 0.30$ and $\Delta m^2 = 1.7\times10^{-5}\,{\rm eV}^2$. The difference of the location of the maximum likelihood and the minimum of X^2 (see Table 3) is due to the determinant $|V_{\rm S}|$ in Eq. (15), that depends on $\tan^2\vartheta$ and Δm^2. In view of the fact that using the maximum likelihood the best fit of the oscillation parameters in the Rates Analysis lies in the same region as the best fit in the Global Analysis (see Section 2.2), a calculation of the allowed regions based on the likelihood [23] may be more robust than the standard calculation based on X^2. We do not present it here because we consider the Bayesian analysis discussed in Section 3 definitely superior.

Frequentist Statistics, whose justification is purely subjective. For example, one may reason in the framework of 2+2 four-neutrino schemes[6] (see [7, 17, 18, 19, 20] and references therein), where transitions of active in sterile neutrinos is predicted in solar or atmospheric neutrino experiments. Since no such transitions have been seen in atmospheric neutrino experiments [54, 55], one could consider reasonable the null hypothesis that the solar neutrino problem is due to practically pure $\nu_e \to \nu_s$ transitions[7].

The interpretation of the value of the likelihood ratio for hypothesis testing is another subjective choice necessary in the application of Frequentist Statistics, since the likelihood does not represent a probability. Usually one chooses an arbitrary value[8], of the order of 0.1% or 1%, below which the null hypothesis is rejected in favor of the alternative hypothesis. Clearly, the large value of the likelihood ratio (14) does not allow to reject the null hypothesis of pure Sterile transitions.

However, we expect better chances to reject the null hypothesis of pure Sterile transitions using for the Super-Kamiokande experiment the energy threshold $T_e^{\rm SK} = 8.6\,{\rm MeV}$, for which the SNO and Super-Kamiokande response functions are approximately equal [5]. Indeed, we find

$$\frac{{\rm Max}_{\tan^2\vartheta,\Delta m^2,\alpha_{\rm C}}\, p^{(\rm S)}({\rm D}(T_e^{\rm SK} = 8.6\,{\rm MeV})|\tan^2\vartheta,\Delta m^2,\alpha_{\rm C})}{{\rm Max}_{\tan^2\vartheta,\Delta m^2,\alpha_{\rm C}}\, p^{(\rm A)}({\rm D}(T_e^{\rm SK} = 8.6\,{\rm MeV})|\tan^2\vartheta,\Delta m^2,\alpha_{\rm C})} = 0.05\,, \qquad (16)$$

that is significantly lower than the value in Eq. (14), but still not sufficient to reject the null hypothesis of pure Sterile transitions.

Hence, we see that in the Rates Analysis of solar neutrino data in terms of neutrino oscillations Frequentist methods are not able to reject the hypothesis of pure Sterile transitions, that are excluded at 3.06σ in a model-independent way [2, 5, 6]. On the other hand, Bayesian Probability Theory allows to assign probabilities to hypotheses and, as we will see in Section 3.1, allows to show clearly that $\nu_e \to \nu_s$ transitions are disfavored with respect to $\nu_e \to \nu_a$ transitions.

Let us determine now the allowed values for the oscillation parameters $\tan^2\vartheta$ and Δm^2 in the case of $\nu_e \to \nu_a$ transitions. As done in Refs. [5, 14], we do not consider $\nu_e \to \nu_s$ transitions because they are excluded at 3.06σ in a model-independent way, as discussed in Refs. [2, 5, 6].

In a standard X^2 analysis the $100\beta\%$ CL regions in the $\tan^2\vartheta$–Δm^2 plane are given by the condition

$$X^2 \leq X^2_{\rm min} + \Delta X^2(\beta)\,,$$

[6] In order to compare Active and Sterile transitions one must work in the framework of a scheme with four or more massive neutrinos. Three neutrinos (ν_e, ν_μ, ν_τ) are not enough, because the existence of sterile neutrinos would be excluded a priori.

[7] A different point of view could be favored by other scientists, as the authors of Ref. [32], where a very interesting 3+1 four neutrino scheme with practically no transitions of active into sterile neutrinos in both solar and atmospheric neutrino experiments has been proposed. In general, in the framework of 3+1 four neutrino schemes there may be or not transitions of active into sterile neutrinos in solar and atmospheric neutrino experiments. Hence, for solar neutrinos one can consider arbitrarily Active transitions as the null hypothesis and Sterile transitions as the alternative hypothesis, or vice versa.

[8] Sometimes the value of this small number can be justified in the asymptotic limit of a large number of observations (see [53]). Clearly this limit has absolutely no interest in the case of solar neutrino experiments.

where β is the Confidence Level (CL) and $\Delta X^2(\beta)$ is the value of X^2 such that the cumulative X^2 distribution for 2 degrees of freedom is equal to β: $\Delta X^2(\beta) = 4.61$, 5.99, 9.21, 11.83 for $\beta = 0.90(1.64\sigma)$, $0.95(1.96\sigma)$, $0.99(2.58\sigma)$, $0.9973(3\sigma)$.

The allowed regions that we obtain with this standard method in the case of $\nu_e \to \nu_a$ transitions are shown in Fig. 1. One can see that, although the minimum of X^2 lies in the VO region, only small areas in the VO region are allowed, because the oscillation probability is very sensitive to variations of Δm^2 and $\tan^2\vartheta$. The allowed Large Mixing Angle (LMA) region is much larger, because the sensitivity of the oscillation probability to variations of Δm^2 and $\tan^2\vartheta$ is weak and the value of X^2 is low ($X^2 = 9.1$ in the local minimum in the LMA region, for $\tan^2\vartheta = 0.34$ and $\Delta m^2 = 2.0 \times 10^{-5}\,\mathrm{eV}^2$). Also the Small Mixing Angle (SMA) and LOW regions are relatively large for the same reason ($X^2 = 10.2$ in the local minimum in the SMA region, for $\tan^2\vartheta = 1.4 \times 10^{-3}$ and $\Delta m^2 = 8.1 \times 10^{-6}\,\mathrm{eV}^2$, and $X^2 = 12.8$ in the local minimum in the LOW region, for $\tan^2\vartheta = 0.60$ and $\Delta m^2 = 1.4 \times 10^{-7}\,\mathrm{eV}^2$). The main effect of the inclusion in the analysis of the CHOOZ data is to limit the LMA region at large CL below $\Delta m^2 \sim 10^{-3}\,\mathrm{eV}^2$ (in Fig. 1, as well as in the following Figs. 2, 3, 4).

2.2 Global Analysis

In our Global Analysis, instead of the total rate of the Super-Kamiokande experiment we consider the data on the Super-Kamiokande day and night electron energy spectra presented in Ref. [56], that contain information on the total rate plus the shape of the energy spectrum. The least-squares function is written as in Eq. (6), with the CHOOZ contribution X^2_{C} given in Eq. (13). The solar contribution X^2_{S} is written as in Eq. (7), but now the indexes j_1, j_2 run from 1 to $N_{\mathrm{S}} = 41$. The indexes $j_1, j_2 = 1, 2, 3$ refer to the first three rates in Table 1. The indexes $j_1, j_2 = 4, \ldots, 22$ and the indexes $j_1, j_2 = 23, \ldots, 41$ refer, respectively, to the data on the Super-Kamiokande day and night electron energy spectra presented in Table III of Ref. [56]. The covariance matrix V_{S} is written as

$$
\begin{aligned}
(V_{\mathrm{S}})_{j_1,j_2} =& \delta_{j_1,j_2}\sigma^2_{j_1} + \delta_{j_1,j_2}\left(\sum_{i_1} R^{(\mathrm{th})}_{i_1,j_1}\Delta\ln C^{(\mathrm{th})}_{i_1,j_1}\right)^2 + \sum_{i_1,i_2} R^{(\mathrm{th})}_{i_1,j_1} R^{(\mathrm{th})}_{i_2,j_2} \sum_k \alpha_{i_1,k}\alpha_{i_2,k}\left(\Delta\ln X_k\right)^2 \\
& + \theta_{j_1-3}\,\theta_{j_2-3}\left[(\sigma^{(\mathrm{sys})}_{\mathrm{cor}})_{j_1}\,(\sigma^{(\mathrm{sys})}_{\mathrm{cor}})_{j_2} + (\sigma^{(\mathrm{sys})}_{\mathrm{unc}})^2_{j_1}\,(\delta_{j_1,j_2-14} + \delta_{j_1,j_2+14})\right] , \qquad (17)
\end{aligned}
$$

with $\theta_j = 1$ for $j > 0$ and $\theta_j = 0$ otherwise. The quantities for $j_1, j_2 \leq 3$ are as in Eq. (8). For $j = 4, \ldots, 41$ we have $\sigma^2_j = (\sigma^{(\mathrm{sta})})^2_j + (\sigma^{(\mathrm{sys})}_{\mathrm{unc}})^2_j$. The statistical uncertainties $(\sigma^{(\mathrm{sta})})_j$ (for $j = 4, \ldots, 41$) are given in the third and fourth columns of Table III in Ref. [56]. The correlated and uncorrelated systematical uncertainties, $(\sigma^{(\mathrm{sys})}_{\mathrm{cor}})_j$ and $(\sigma^{(\mathrm{sys})}_{\mathrm{unc}})_j$ (for $j = 4, \ldots, 41$), are given, respectively, by $R^{(\mathrm{ex})}_j\,\delta_{j,\mathrm{cor}}$ and $R^{(\mathrm{ex})}_j\,\delta_{j,\mathrm{unc}}$, with $R^{(\mathrm{ex})}_j$ listed in the third and fourth columns of Table III in Ref. [56] for $j = 4, \ldots, 22$ (day spectrum) and $j = 23, \ldots, 41$ (night spectrum). The values of $\delta_{j,\mathrm{cor}}$ and $\delta_{j,\mathrm{unc}}$ are listed, respectively, in the fifth and sixth columns of Table III in Ref. [56]. For both $\delta_{j,\mathrm{cor}}$ and $\delta_{j,\mathrm{unc}}$ we took the bigger between the positive and negative values given in Table III of Ref. [56]. In Eq. (17) we assumed that the systematic uncertainties of the day and night bins with the same energy are fully correlated.

The values of the minimum X^2_{min} of the least-squares function in the Global Analysis in terms of $\nu_e \to \nu_a$ and $\nu_e \to \nu_s$ oscillations are given, respectively, in the third and fourth row

of Table 3. One can see that $X^2_{\rm min}$ lies in the LMA region in the case of Active transitions, whereas it lies in the VO region in the case of Sterile transitions. Again we see that the standard goodness of fit test is not able to exclude pure Sterile transitions. As in the case of the Rates Analysis, the fact that the expected value of $X^2_{\rm min}$ is the number of degrees of freedom could induce to believe that Sterile transitions are favored over Active transitions, or at least not disfavored, in contradiction with the model-independent exclusion at 3.06σ of pure Sterile transitions discussed in Refs. [2, 5, 6]. The reason of the low values of $X^2_{\rm min}$ with respect to the number of degrees of freedom is the high number of Super-Kamiokande and CHOOZ energy bins whose data do not fluctuate enough. This fact could be due to chance or to an overestimation of systematic uncertainties.

However, in the Global Analysis the likelihood test allows to reject the null hypothesis of pure Sterile transitions in favor of the alternative hypothesis of pure Active transitions. Indeed, we find

$$\frac{\mathrm{Max}_{\tan^2\vartheta,\Delta m^2,\alpha_{\rm C}}\, p^{(\rm S)}(\rm D|\,\tan^2\vartheta,\Delta m^2,\alpha_{\rm C})}{\mathrm{Max}_{\tan^2\vartheta,\Delta m^2,\alpha_{\rm C}}\, p^{(\rm A)}(\rm D|\,\tan^2\vartheta,\Delta m^2,\alpha_{\rm C})} = 3\times 10^{-4}\,, \tag{18}$$

that is small enough.

Assuming that pure Sterile transitions are excluded, we present in Fig. 2 the allowed regions in the $\tan^2\vartheta$–Δm^2 plane for Active transitions. One can see that there is no allowed SMA region, in agreement with the results presented in Refs. [5, 14], and the allowed VO regions are very small. The local minimum in the LOW region has $X^2 = 42.3$, for $\tan^2\vartheta = 0.64$ and $\Delta m^2 = 1.4\times 10^{-7}\,\mathrm{eV}^2$, and the local minimum in the VO region has $X^2 = 44.5$, for $\tan^2\vartheta = 0.38, 2.6$ and $\Delta m^2 = 4.9\times 10^{-10}\,\mathrm{eV}^2$.

3 Bayesian Analysis

In this Section we present our results on the fit of solar neutrino data in the framework of Bayesian Probability Theory. In Section 3.1 we compare the probabilities of $\nu_e \to \nu_a$ and $\nu_e \to \nu_s$ transitions, and in Section 3.2 we calculate the Bayesian allowed regions (credible regions) for the oscillation parameters Δm^2 and $\tan^2\vartheta$ in the case of $\nu_e \to \nu_a$ transitions.

Bayes Theorem allows to calculate the *posterior probability distribution function* $p(\mathrm{T}, \tan^2\vartheta, \Delta m^2|\mathrm{D},\mathrm{I})$, where T indicates the type of transitions: T = A for $\nu_e \to \nu_a$ transitions (Active), and T = S for $\nu_e \to \nu_s$ transitions (Sterile). Here D represents the data and I represent all the background information and assumptions on solar physics, neutrino physics, etc. For our analysis Bayes Theorem can be written as

$$p(\mathrm{T}, \tan^2\vartheta, \Delta m^2|\mathrm{D},\mathrm{I}) = \frac{p(\mathrm{D}|\mathrm{T}, \tan^2\vartheta, \Delta m^2, \mathrm{I})\, p(\mathrm{T}, \tan^2\vartheta, \Delta m^2|\mathrm{I})}{p(\mathrm{D}|\mathrm{I})}\,, \tag{19}$$

where $p(\mathrm{D}|\mathrm{T}, \tan^2\vartheta, \Delta m^2, \mathrm{I})$ is the *likelihood function* and $p(\mathrm{T}, \tan^2\vartheta, \Delta m^2|\mathrm{I})$ is the *prior probability distribution function* (the inclusion of background information and assumptions is necessary because in Bayesian Probability Theory, as in real life, all probabilities are conditional). The probability $p(\mathrm{D}|\mathrm{I})$ is known as *global likelihood* and acts as a normalization constant.

Assuming a normal distribution of statistical and systematic errors, the likelihood function is given by

$$p(\mathrm{D}|\mathrm{T},\tan^2\vartheta,\Delta m^2,\mathrm{I}) = \frac{e^{-X^2_{\mathrm{S}}/2}}{(2\pi)^{N_{\mathrm{S}}/2}\sqrt{|V_{\mathrm{S}}|}} \int \mathrm{d}\alpha_{\mathrm{C}} \frac{e^{-X^2_{\mathrm{C}}/2}}{(2\pi)^{N_{\mathrm{C}}/2}\sqrt{|V_{\mathrm{C}}|}}\,, \tag{20}$$

where we have marginalized the nuisance parameter α_{C}. Here N_{S} is the number of solar data points ($N_{\mathrm{S}} = 4$ in the Rates Analysis and $N_{\mathrm{S}} = 41$ in the Global Analysis) and $N_{\mathrm{C}} = 14$ is the number of CHOOZ data points. X^2_{S} is the solar least-squares function and V_{S} is the corresponding covariance matrix, whose calculation in the Rates Analysis and in the Global Analysis is explained, respectively, in Sections 2.1 and 2.2. X^2_{C} is the CHOOZ least-squares function and V_{C} is the corresponding covariance matrix, whose calculation is explained in Section 2.1.

The prior probability distribution function can be written as

$$p(\mathrm{T},\tan^2\vartheta,\Delta m^2|\mathrm{I}) = p(\tan^2\vartheta,\Delta m^2|\mathrm{T},\mathrm{I})\,p(\mathrm{T}|\mathrm{I})\,, \tag{21}$$

where $p(\mathrm{T}|\mathrm{I})$ is the prior probability of $\nu_e \to \nu_a$ ($\mathrm{T} = \mathrm{A}$) or $\nu_e \to \nu_s$ transitions ($\mathrm{T} = \mathrm{S}$), and $p(\tan^2\vartheta,\Delta m^2|\mathrm{T},\mathrm{I})$ is the prior probability distribution function of the parameters $\tan^2\vartheta$ and Δm^2 given T and I.

The prior probability distribution function $p(\tan^2\vartheta,\Delta m^2|\mathrm{T},\mathrm{I})$ quantifies the prior knowledge on the parameters $\tan^2\vartheta$ and Δm^2. Assuming neutrino mixing (included in I), for both $\mathrm{T} = \mathrm{A}$ and $\mathrm{T} = \mathrm{S}$ we know that solar neutrino data are sensitive to several different order of magnitude of $\tan^2\vartheta$ and Δm^2, through vacuum oscillations for $\Delta m^2 \lesssim 10^{-8}\,\mathrm{eV}^2$ and large mixing angles or resonant MSW transitions for $10^{-8}\,\mathrm{eV}^2 \lesssim \Delta m^2 \lesssim 10^{-3}\,\mathrm{eV}^2$ and $10^{-4} \lesssim \tan^2\vartheta \lesssim 10$. Therefore, the most reasonable non-informative prior probability distribution function, that we will use in the following, is a flat distribution in the $\log(\tan^2\vartheta)$–$\log(\Delta m^2)$ plane for both $\mathrm{T} = \mathrm{A}$ and $\mathrm{T} = \mathrm{S}$. In this case, using Eq. (21), Eq. (19) becomes

$$p(\mathrm{T},\tan^2\vartheta,\Delta m^2|\mathrm{D},\mathrm{I}) = \frac{p(\mathrm{D}|\mathrm{T},\tan^2\vartheta,\Delta m^2,\mathrm{I})\,p(\mathrm{T}|\mathrm{I})}{\displaystyle\sum_{\mathrm{T=A,S}} \int \mathrm{dlog}(\tan^2\vartheta)\,\mathrm{dlog}(\Delta m^2)\,p(\mathrm{D}|\mathrm{T},\tan^2\vartheta,\Delta m^2,\mathrm{I})\,p(\mathrm{T}|\mathrm{I})}\,, \tag{22}$$

where we have expressed the global likelihood $p(\mathrm{D}|\mathrm{I})$ as the appropriate normalization constant and all probabilities are calculated integrating $p(\mathrm{T},\tan^2\vartheta,\Delta m^2|\mathrm{D},\mathrm{I})$ over $\mathrm{dlog}(\tan^2\vartheta)\,\mathrm{dlog}(\Delta m^2)$.

3.1 Active Or Sterile?

In this Section we confront the probabilities of Active $\nu_e \to \nu_a$ and Sterile $\nu_e \to \nu_s$ transitions using the relation

$$p(\mathrm{T}|\mathrm{D},\mathrm{I}) = \int \mathrm{dlog}(\tan^2\vartheta)\,\mathrm{dlog}(\Delta m^2)\,p(\mathrm{T},\tan^2\vartheta,\Delta m^2|\mathrm{D},\mathrm{I})\,. \tag{23}$$

From Eq. (22), the ratio of the probabilities of Sterile and Active transitions is given by

$$\frac{p(\mathrm{S}|\mathrm{D},\mathrm{I})}{p(\mathrm{A}|\mathrm{D},\mathrm{I})} = \frac{\int \mathrm{dlog}(\tan^2\vartheta)\,\mathrm{dlog}(\Delta m^2)\,p(\mathrm{D}|\mathrm{S},\tan^2\vartheta,\Delta m^2,\mathrm{I})}{\int \mathrm{dlog}(\tan^2\vartheta)\,\mathrm{dlog}(\Delta m^2)\,p(\mathrm{D}|\mathrm{A},\tan^2\vartheta,\Delta m^2,\mathrm{I})}\,\frac{p(\mathrm{S}|\mathrm{I})}{p(\mathrm{A}|\mathrm{I})}\,. \tag{24}$$

Notice that the ratio of the prior probabilities of Sterile and Active transitions factorizes out. Since we do not have any prior preference for Sterile or Active transitions, we take their prior probabilities as equal, leading to

$$\frac{p(\mathrm{S}|\mathrm{D},\mathrm{I})}{p(\mathrm{A}|\mathrm{D},\mathrm{I})} = \frac{\int \mathrm{dlog}(\tan^2\vartheta)\,\mathrm{dlog}(\Delta m^2)\,p(\mathrm{D}|\mathrm{S},\tan^2\vartheta,\Delta m^2,\mathrm{I})}{\int \mathrm{dlog}(\tan^2\vartheta)\,\mathrm{dlog}(\Delta m^2)\,p(\mathrm{D}|\mathrm{A},\tan^2\vartheta,\Delta m^2,\mathrm{I})}\,. \tag{25}$$

Our result in the Rates Analysis ($(\mathrm{D},\mathrm{I}) = \mathrm{RatesAnalysis}$) is

$$\frac{p(\mathrm{S}|\mathrm{RatesAnalysis})}{p(\mathrm{A}|\mathrm{RatesAnalysis})} = 2.8\times 10^{-2}\,. \tag{26}$$

It is clear that Sterile transitions are disfavored with respect to Active transitions, in agreement with the model-independent exclusion at 3.06σ of pure Sterile transitions [2, 5, 6]. From the discussion in Section 2.1, it is clear that the incompatibility of Sterile transitions with the data should be enhanced by choosing for the Super-Kamiokande experiment the energy threshold $T_e^{\mathrm{SK}} = 8.6\,\mathrm{MeV}$, for which the SNO and Super-Kamiokande response functions are approximately equal [5]. Indeed, we find

$$\frac{p(\mathrm{S}|\mathrm{RatesAnalysis},T_e^{\mathrm{SK}}=8.6\,\mathrm{MeV})}{p(\mathrm{A}|\mathrm{RatesAnalysis},T_e^{\mathrm{SK}}=8.6\,\mathrm{MeV})} = 1.5\times 10^{-2}\,. \tag{27}$$

Notice that, although the number in Eq. (27) is comparable with the one in the likelihood ratio (16), the interpretation is very different. Here we have a ratio of probabilities of hypotheses and a very small ratio means that the probability of Sterile transitions is much smaller than that of Active transitions. No such interpretation exist for the likelihood ratio in the framework of Frequentist Statistics, in which the null hypothesis hypothesis can be either accepted or rejected in favor of an alternative hypothesis on the basis of the comparison of the value of the likelihood ratio with a very small fixed number chosen arbitrarily in advance (see footnote 8).

Our result in the Global Analysis ($(\mathrm{D},\mathrm{I}) = \mathrm{GlobalAnalysis}$) is even stronger:

$$\frac{p(\mathrm{S}|\mathrm{GlobalAnalysis})}{p(\mathrm{A}|\mathrm{GlobalAnalysis})} = 4\times 10^{-4}\,, \tag{28}$$

that practically excludes Sterile transitions with respect to Active transitions.

Hence, the Bayesian analysis of solar neutrino data shows that Sterile transitions are strongly disfavored with respect to Active transitions, in agreement with the model-independent exclusion at 3.06σ of pure Sterile transitions [2, 5, 6]. We see that Bayesian Probability Theory gives an unambiguous and correct result in the comparison of Active and Sterile transitions in both the Rates and Global Analysis, contrary to the popular goodness

of fit test used in traditional analyses of solar neutrino data and the likelihood ratio test in the Rates Analysis, as shown in Section 2.

This better performance of Bayesian Probability Theory in model comparison is first of all due to the fact that in Bayesian Probability Theory as in real life one can assign probabilities to hypotheses and discuss which hypothesis is more or less favored in comparison with others, whereas in Frequentist Statistics one is only allowed to either accept or reject an hypothesis. Secondly, the judgment of an hypothesis in the framework of Bayesian Probability Theory is more robust than in Frequentist Statistics because Bayesian Probability Theory allows to estimate the likelihood of a model not only from the best-fit point of its parameter space as in Frequentist methods, but from the performance of the model averaged over all its parameter space. Thirdly, in the framework of Bayesian Probability Theory different hypotheses are fairly compared assigning to them the same prior, whereas in the likelihood ratio test it is required to choose a null hypothesis and an alternative hypothesis, that are treated quite differently.

Notice that the Bayesian method does not suffer any problem from the inclusion of the numerous bins of the CHOOZ and Super-Kamiokande electron energy spectra, contrary to the least-squares method discussed in Section 2.

3.2 Credible Regions

In this Section we present the results of our calculation of Bayesian *credible regions* (also known as *highest posterior density regions*) in the plane of the oscillation parameters $\tan^2\vartheta$ and Δm^2 for Active transitions, that are strongly favored over Sterile transitions, as shown in Section 3.1. The credible regions are so-called in order to distinguish them from the "confidence regions" calculated in the framework of Frequentist Statistics. Credible regions contain a specified fraction of the posterior probability and all values of the parameters inside the credible regions have higher probability than those outside.

The posterior probability distribution function for the oscillation parameters $\tan^2\vartheta$ and Δm^2 in the case of Active transitions is given by

$$p(\tan^2\vartheta, \Delta m^2|\mathrm{A}, \mathrm{D}, \mathrm{I}) = \frac{p(\mathrm{A}, \tan^2\vartheta, \Delta m^2|\mathrm{D}, \mathrm{I})}{p(\mathrm{A}|\mathrm{D}, \mathrm{I})}\,. \tag{29}$$

Assuming Active transitions implies that we take the prior probability of Active transitions to be unity:

$$p(\mathrm{A}|\mathrm{I}) = 1\,, \tag{30}$$

that implies $p(\mathrm{S}|\mathrm{I}) = 0$. Therefore, we have

$$p(\mathrm{D}|\mathrm{I}) = p(\mathrm{D}, \mathrm{A}|\mathrm{I}) + p(\mathrm{D}, \mathrm{S}|\mathrm{I}) = p(\mathrm{D}|\mathrm{A}, \mathrm{I})\, p(\mathrm{A}|\mathrm{I}) + p(\mathrm{D}|\mathrm{S}, \mathrm{I})\, p(\mathrm{S}|\mathrm{I}) = p(\mathrm{D}|\mathrm{A}, \mathrm{I})\,, \tag{31}$$

and

$$p(\mathrm{A}|\mathrm{D}, \mathrm{I}) = \frac{p(\mathrm{D}|\mathrm{A}, \mathrm{I})\, p(\mathrm{A}|\mathrm{I})}{p(\mathrm{D}|\mathrm{I})} = 1\,. \tag{32}$$

From Eqs. (22), (29), (30) and (32) we obtain

$$p(\tan^2\vartheta, \Delta m^2|\mathrm{A},\mathrm{D},\mathrm{I}) = \frac{p(\mathrm{D}|\mathrm{A},\tan^2\vartheta,\Delta m^2,\mathrm{I})}{\displaystyle\int \mathrm{dlog}(\tan^2\vartheta)\,\mathrm{dlog}(\Delta m^2)\,p(\mathrm{D}|\mathrm{A},\tan^2\vartheta,\Delta m^2,\mathrm{I})}\,. \tag{33}$$

Using the expression (20) with T = A for $p(\mathrm{D}|\mathrm{A},\tan^2\vartheta,\Delta m^2,\mathrm{I})$, we obtained the credible regions with 90%, 95%, 99% and 99.73% posterior probability shown in Fig. 3 for the Rates Analysis and in Fig. 4 for the Global Analysis. One can see that these regions are similar but larger than the corresponding allowed regions obtained with the standard least-squares analysis presented in Figs. 1 and 2. Let us emphasize, however, that the meaning of Bayesian and Frequentist regions is quite different and a direct comparison is meaningless.

Bayesian Probability Theory allows to calculate the relative probabilities of the SMA, LMA, LOW and VO regions. The posterior probability that the true values of the oscillation parameters lie in a region R, with R = SMA, LMA, LOW, VO, is given by

$$p(\mathrm{R}|\mathrm{A},\mathrm{D},\mathrm{I}) = \int_{\mathrm{R}} \mathrm{dlog}(\tan^2\vartheta)\,\mathrm{dlog}(\Delta m^2)\,p(\tan^2\vartheta,\Delta m^2|\mathrm{A},\mathrm{D},\mathrm{I})\,, \tag{34}$$

where the integration is performed over the appropriate ranges of the parameters given in Eqs. (2)–(5).

In the Rates Analysis we found

$$\begin{aligned} &p(\mathrm{LMA}|\mathrm{A},\mathrm{D},\mathrm{I}) = 0.72\,,\\ &p(\mathrm{VO}|\mathrm{A},\mathrm{D},\mathrm{I}) = 0.12\,,\\ &p(\mathrm{SMA}|\mathrm{A},\mathrm{D},\mathrm{I}) = 0.10\,,\\ &p(\mathrm{LOW}|\mathrm{A},\mathrm{D},\mathrm{I}) = 0.06\,, \end{aligned} \tag{35}$$

and in the Global Analysis

$$\begin{aligned} &p(\mathrm{LMA}|\mathrm{A},\mathrm{D},\mathrm{I}) = 0.85\,,\\ &p(\mathrm{LOW}|\mathrm{A},\mathrm{D},\mathrm{I}) = 0.13\,,\\ &p(\mathrm{VO}|\mathrm{A},\mathrm{D},\mathrm{I}) = 0.02\,,\\ &p(\mathrm{SMA}|\mathrm{A},\mathrm{D},\mathrm{I}) = 10^{-4}\,. \end{aligned} \tag{36}$$

Hence, the LMA region is favored in the Global Analysis as well as in the Rates Analysis (see Ref. [15] for an explanation of the physical reason). This consistency in the Bayesian analysis of solar neutrino data is very interesting and promising for future experiments that plan to explore the LMA region with terrestrial experiments [57, 58].

3.3 Marginal Bayesian Distributions

In this Section we marginalize the posterior probability (33) in order to derive the separate posterior probability distributions for $\tan^2\vartheta$ and Δm^2:

$$p(\tan^2\vartheta|\mathrm{A},\mathrm{D},\mathrm{I}) = \int \mathrm{dlog}(\Delta m^2)\,p(\tan^2\vartheta,\Delta m^2|\mathrm{A},\mathrm{D},\mathrm{I})\,, \tag{37}$$

$$p(\Delta m^2|\mathrm{A},\mathrm{D},\mathrm{I}) = \int \mathrm{dlog}(\tan^2\vartheta)\,p(\tan^2\vartheta,\Delta m^2|\mathrm{A},\mathrm{D},\mathrm{I})\,. \tag{38}$$

The posterior probability distributions that we obtained in the Rates Analysis are shown in Figs. 5 and 6 and those that we obtained in the Global Analysis are shown in Figs. 7 and 8.

From Fig. 5 one can see that in the Rates Analysis there are two peaks of the posterior probability distribution for $\tan^2\vartheta$: one at small mixing angles, $\tan^2\vartheta \sim 10^{-3}$, and one for large mixing angles, $\tan^2\vartheta \sim 0.3$. However, large mixing angles are strongly favored, as one can see calculating the corresponding probability:

$$p(0.1 < \tan^2\vartheta < 10|\mathrm{A},\mathrm{D},\mathrm{I}) = 0.90\,. \tag{39}$$

In the case of the Global Analysis, Fig. 7 shows that there is only one peak for the posterior probability distribution for $\tan^2\vartheta$ at large mixing angles, with probability close to unity.

Figure 6 shows that in the Rates Analysis the posterior probability distribution of Δm^2 has a large and high peak for $2\times 10^{-6}\,\mathrm{eV}^2 \lesssim \Delta m^2 \lesssim 10^{-3}\,\mathrm{eV}^2$, a small and low peak for $\Delta m^2 \sim 10^{-7}\,\mathrm{eV}^2$, and several sharp peaks for $\Delta m^2 \lesssim 10^{-8}\,\mathrm{eV}^2$ (due to the rapid oscillations of the transition probability in vacuum as a function of Δm^2). A calculation of the corresponding probabilities shows that large values of Δm^2 are favored:

$$\begin{aligned}
&p(2\times 10^{-6}\,\mathrm{eV}^2 < \Delta m^2 < 10^{-3}\,\mathrm{eV}^2|\mathrm{A},\mathrm{D},\mathrm{I}) = 0.82\,,\\
&p(10^{-8}\,\mathrm{eV}^2 < \Delta m^2 < 2\times 10^{-6}\,\mathrm{eV}^2|\mathrm{A},\mathrm{D},\mathrm{I}) = 0.06\,,\\
&p(\Delta m^2 < 10^{-8}\,\mathrm{eV}^2|\mathrm{A},\mathrm{D},\mathrm{I}) = 0.12\,.
\end{aligned} \tag{40}$$

From Fig. 8 one can see that in the Global Analysis large values of Δm^2 are even more favored than in the Rates Analysis and very small values are strongly disfavored. Indeed, we obtained the probabilities

$$\begin{aligned}
&p(2\times 10^{-6}\,\mathrm{eV}^2 < \Delta m^2 < 10^{-3}\,\mathrm{eV}^2|\mathrm{A},\mathrm{D},\mathrm{I}) = 0.85\,,\\
&p(10^{-8}\,\mathrm{eV}^2 < \Delta m^2 < 2\times 10^{-6}\,\mathrm{eV}^2|\mathrm{A},\mathrm{D},\mathrm{I}) = 0.13\,,\\
&p(\Delta m^2 < 10^{-8}\,\mathrm{eV}^2|\mathrm{A},\mathrm{D},\mathrm{I}) = 0.02\,.
\end{aligned} \tag{41}$$

4 Conclusions

In this paper we have presented the results of a Bayesian analysis of solar neutrino data, including the recently published rate of CC interactions in the SNO experiment [2], and the data of the CHOOZ experiment [31], that exclude large values of the mixing angle for $\Delta m^2 \gtrsim 10^{-3}\,\mathrm{eV}^2$. We have considered $\nu_e \to \nu_a$ oscillations, with $a = \mu, \tau$, and $\nu_e \to \nu_s$ oscillations, where ν_s is a sterile neutrino. We have shown in Section 3.1 that the Bayesian analysis implies that $\nu_e \to \nu_s$ transitions are strongly disfavored with respect to $\nu_e \to \nu_a$ transitions, in agreement with the model-independent 3.06σ exclusion of pure $\nu_e \to \nu_s$ transitions discussed in Refs. [2, 5, 6].

We have also presented, in Section 2, the results of a standard least-squares analysis of solar neutrino data and we have shown that the standard goodness of fit test is not able to exclude pure $\nu_e \to \nu_s$ transitions. The likelihood ratio test allows to reject the null hypothesis of pure $\nu_e \to \nu_s$ transitions in favor of $\nu_e \to \nu_a$ transitions only in the Global Analysis.

In Section 3.2 we have presented the results of our calculation of Bayesian credible regions in the plane of the oscillation parameters $\tan^2\vartheta$ and Δm^2 for $\nu_e \to \nu_a$ transitions (Figs. 3 and 4). The Bayesian credible regions are significantly larger than the corresponding least-squares allowed region (Figs. 1 and 2), presented in Sections 2.1 and 2.2. However, it is always necessary to keep in mind that a direct comparison of Bayesian and Frequentist regions is meaningless, because they have different properties due to the different definitions of probability in Bayesian Probability Theory and Frequentist Statistics.

Bayesian Probability Theory allows to calculate the probability of separate regions in the plane of the oscillation parameters $\tan^2\vartheta$ and Δm^2. We found in the Global Analysis that the Large Mixing Angle (LMA) region is strongly favored by the data (85% probability), the LOW region has some small chance (13% probability), the Vacuum Oscillation (VO) region is almost excluded (2% probability) and the Small Mixing Angle (SMA) region is practically excluded (0.01% probability). Also the Rates Analysis favors the LMA region.

We have also presented in Section 3.3 the marginal posterior probability distributions for $\tan^2\vartheta$ and Δm^2. In the Global Analysis the data imply large mixing almost with certainty and large values of Δm^2 are favored ($2 \times 10^{-6}\,\mathrm{eV}^2 < \Delta m^2 < 10^{-3}\,\mathrm{eV}^2$ with 85% probability). Also in the Rates Analysis large mixing and large values of Δm^2 are favored.

These indications in favor of large mixing and large values for Δm^2 are very encouraging for future terrestrial experiments as KAMLAND [57] and BOREXINO [57, 58] that have the possibility to explore this region of parameter space.

In conclusion, we want to emphasize the better performance shown in this paper of Bayesian Probability Theory with respect to Frequentist Statistics in the analysis of solar neutrino data. In particular, the Bayesian analysis of solar neutrino data is able to disfavor clearly Sterile transitions with respect to Active ones, does not suffer any problem from the inclusion in the analysis of the numerous bins of the CHOOZ and Super-Kamiokande electron energy spectra, allows to reach the same conclusion on the determination of the most favored values of the oscillation parameters in both the Rates and Global Analysis.

References

[1] J. N. Bahcall, Nucl. Phys. Proc. Suppl. **91**, 9 (2000), hep-ph/0009044.

[2] SNO, Q. R. Ahmad *et al.*, (2001), nucl-ex/0106015.

[3] J. N. Bahcall, M. H. Pinsonneault, and S. Basu, Astrophys. J. **555**, 990 (2001), astro-ph/0010346.

[4] SuperKamiokande, S. Fukuda *et al.*, Phys. Rev. Lett. **86**, 5651 (2001), hep-ex/0103032.

[5] G. L. Fogli, E. Lisi, D. Montanino, and A. Palazzo, (2001), hep-ph/0106247.

[6] C. Giunti, (2001), hep-ph/0107310.

[7] S. M. Bilenky, C. Giunti, and W. Grimus, Prog. Part. Nucl. Phys. **43**, 1 (1999), hep-ph/9812360.

[8] Super-Kamiokande, Y. Fukuda *et al.*, Phys. Rev. Lett. **81**, 1562 (1998), hep-ex/9807003.

[9] B. T. Cleveland *et al.*, Astrophys. J. **496**, 505 (1998).

[10] GALLEX, W. Hampel *et al.*, Phys. Lett. **B447**, 127 (1999).

[11] SAGE, V. N. Gavrin, Nucl. Phys. Proc. Suppl. **91**, 36 (2001).

[12] GNO, M. Altmann *et al.*, Phys. Lett. **B490**, 16 (2000), hep-ex/0006034.

[13] J. N. Bahcall, M. C. Gonzalez-Garcia, and C. Pena-Garay, (2001), hep-ph/0106258.

[14] A. Bandyopadhyay, S. Choubey, S. Goswami, and K. Kar, (2001), hep-ph/0106264.

[15] V. Berezinsky and M. Lissia, (2001), hep-ph/0108108.

[16] V. Barger, D. Marfatia, and K. Whisnant, (2001), hep-ph/0106207.

[17] D. Dooling, C. Giunti, K. Kang, and C. W. Kim, Phys. Rev. **D61**, 073011 (2000), hep-ph/9908513.

[18] C. Giunti, M. C. Gonzalez-Garcia, and C. Pena-Garay, Phys. Rev. **D62**, 013005 (2000), hep-ph/0001101.

[19] C. Giunti and M. Laveder, JHEP **02**, 001 (2001), hep-ph/0010009.

[20] M. C. Gonzalez-Garcia, M. Maltoni, and C. Pena-Garay, (2001), hep-ph/0105269.

[21] M. V. Garzelli and C. Giunti, (2000), hep-ph/0007155.

[22] P. Creminelli, G. Signorelli, and A. Strumia, (2001), hep-ph/0102234.

[23] M. V. Garzelli and C. Giunti, (2001), hep-ph/0104085.

[24] H. Jeffreys, *Theory of Probability* (Oxford University Press, New York, USA, 1961), First published in 1939.

[25] T. J. Loredo, *From Laplace to Supernova SN 1987A: Bayesian Inference in Astrophysics*, in Maximum-Entropy and Bayesian Methods, Dartmouth, 1989, ed. P. Fougere, Kluwer Academic Publishers, Dordrecht, The Netherlands, 1990, pp. 81–142, http://astrosun.tn.cornell.edu/staff/loredo/bayes/tjl.html.

[26] T. J. Loredo, *The Promise of Bayesian Inference for Astrophysics*, in Statistical Challenges in Modern Astronomy, ed. E.D. Feigelson and G.J. Babu, Springer-Verlag, New York, 1992, pp. 275–297, http://astrosun.tn.cornell.edu/staff/loredo/bayes/tjl.html.

[27] E. T. Jaynes, *Probability Theory: The Logic of Science* (Fragmentary Edition, June 1994), http://bayes.wustl.edu/etj/prob.html.

[28] G. D'Agostini, CERN Yellow Report **99-03** (1999).

[29] S. M. Bilenky and C. Giunti, Phys. Lett. **B444**, 379 (1998), hep-ph/9802201.

[30] G. L. Fogli, E. Lisi, D. Montanino, and A. Palazzo, Phys. Rev. **D62**, 013002 (2000), hep-ph/9912231.

[31] M. Apollonio *et al.* (CHOOZ Coll.), Phys. Lett. B **466**, 415 (1999), hep-ex/9907037.

[32] V. Barger, B. Kayser, J. Learned, T. Weiler, and K. Whisnant, Phys. Lett. **B489**, 345 (2000), hep-ph/0008019.

[33] G. L. Fogli and E. Lisi, Astropart. Phys. **3**, 185 (1995).

[34] M. V. Garzelli and C. Giunti, Phys. Lett. **B488**, 339 (2000), hep-ph/0006026.

[35] J.N. Bahcall, WWW page: http://www.sns.ias.edu/~jnb/.

[36] S. Nakamura, T. Sato, V. Gudkov, and K. Kubodera, Phys. Rev. **C63**, 034617 (2001), nucl-th/0009012.

[37] K. Kubodera, WWW page: http://nuc003.psc.sc.edu/~kubodera/NU-D-NSGK.

[38] S.P. Mikheyev and A.Yu. Smirnov, Yad. Fiz. **42**, 1441 (1985) [Sov. J. Nucl. Phys. **42**, 913 (1985)]; Il Nuovo Cim. C **9**, 17 (1986); L. Wolfenstein, Phys. Rev. D **17**, 2369 (1978); Phys. Rev. D **20**, 2634 (1979).

[39] A. Friedland, Phys. Rev. Lett. **85**, 936 (2000), hep-ph/0002063.

[40] G. L. Fogli, E. Lisi, D. Montanino, and A. Palazzo, Phys. Rev. **D62**, 113004 (2000), hep-ph/0005261.

[41] E. Lisi, A. Marrone, D. Montanino, A. Palazzo, and S. T. Petcov, Phys. Rev. **D63**, 093002 (2001), hep-ph/0011306.

[42] M. C. Gonzalez-Garcia and C. Pena-Garay, Nucl. Phys. Proc. Suppl. **91**, 80 (2000), hep-ph/0009041.

[43] S. T. Petcov, Phys. Lett. **B200**, 373 (1988).

[44] T. K. Kuo and J. Pantaleone, Rev. Mod. Phys. **61**, 937 (1989).

[45] Q. Y. Liu, M. Maris, and S. T. Petcov, Phys. Rev. **D56**, 5991 (1997), hep-ph/9702361.

[46] S. T. Petcov, Phys. Lett. **B434**, 321 (1998), hep-ph/9805262.

[47] E. K. Akhmedov, Nucl. Phys. **B538**, 25 (1999), hep-ph/9805272.

[48] M. V. Chizhov and S. T. Petcov, Phys. Rev. Lett. **83**, 1096 (1999), hep-ph/9903399.

[49] M.V. Chizhov and S.T. Petcov, hep-ph/9903424.

[50] M. Apollonio *et al.* (CHOOZ Coll.), Phys. Lett. B **420**, 397 (1998), hep-ex/9711002.

[51] F. L. Villante, G. Fiorentini, and E. Lisi, Phys. Rev. **D59**, 013006 (1999), hep-ph/9807360.

[52] G. L. Fogli, E. Lisi, A. Palazzo, and F. L. Villante, Phys. Rev. **D63**, 113016 (2001), hep-ph/0102288.

[53] W. Eadie, D. Drijard, F. James, M. Roos, and B. Sadoulet, *Statistical Methods in Experimental Physics* (North Holland, Amsterdam, 1971).

[54] Super-Kamiokande, S. Fukuda *et al.*, Phys. Rev. Lett. **85**, 3999 (2000), hep-ex/0009001.

[55] F. Ronga (Macro Coll.), Talk presented at NOW2000, Otranto, Italy, September 2000 (http://www.ba.infn.it/~now2000).

[56] SuperKamiokande, S. Fukuda *et al.*, hep-ex/0103032.

[57] KamLAND, A. Piepke, Nucl. Phys. Proc. Suppl. **91**, 99 (2001).

[58] BOREXINO, G. Ranucci *et al.*, Nucl. Phys. Proc. Suppl. **91**, 58 (2001).

Detection Material and Process	Data
^{37}Cl: $\nu_e + {}^{37}\mathrm{Cl} \to {}^{37}\mathrm{Ar} + e^-$ (Homestake [9])	$2.56 \pm 0.23\,\mathrm{SNU}$
^{71}Ga: $\nu_e + {}^{71}\mathrm{Ga} \to {}^{71}\mathrm{Ge} + e^-$ (GALLEX [10] + GNO [12] + SAGE [11])	$74.7 \pm 5.1\,\mathrm{SNU}$
D_2O: $\nu_e + d \to p + p + e^-$ (SNO [2])	0.347 ± 0.028
H_2O: $\nu + e^- \to \nu + e^-$ (Super-Kamiokande [4])	0.459 ± 0.017

Table 1: The rates measured in solar neutrino experiments. The rates of the Homestake and GALLEX+SAGE+GNO experiments are expressed in SNU units ($1\,\mathrm{SNU} \equiv 10^{-36}\,\mathrm{events\,atom^{-1}\,s^{-1}}$), whereas the results of the Kamiokande and SNO experiments are expressed in terms of the ratio of the experimental rate and the BP2000 Standard Solar Model prediction [3]. The statistical and systematic uncertainties have been added in quadrature. The GALLEX+SAGE+GNO rate is a weighted average of the GALLEX+GNO rate reported in Ref. [12] and the SAGE rate reported in Ref. [11]. The rate of the SNO experiment is that measured through CC weak interactions.

i	1 *pp*	2 *pep*	3 *hep*	4 Be	5 B	6 N	7 O	8 F
$\Delta\ln\Phi_i^{\mathrm{SSM}}$	0.010	0.016	0.033	0.100	0.176	0.184	0.209	0.239

Table 2: Relative uncertainties $\Delta\ln\Phi_i^{\mathrm{SSM}}$ of the neutrino fluxes obtained with Eq. (10). They are in good agreement with those presented in Table 7 of Ref. [3].

Analysis	X^2_{min}	$\tan^2\vartheta$	Δm^2 (eV^2)	n.d.f.	g.o.f.
Active Rates	8.8	$0.31, 3.2$	7.7×10^{-11}	15	89%
Sterile Rates	11.3	$0.36, 2.8$	1.1×10^{-10}	15	73%
Active Global	38.7	0.38	6.3×10^{-5}	52	91%
Sterile Global	53.7	$0.36, 2.8$	4.9×10^{-10}	52	41%

Table 3: Minima X^2_{min} of the least-squares function X^2 for $\nu_e \to \nu_a$ (Active) or $\nu_e \to \nu_s$ (Sterile) in the Rates Analysis of Section 2.1 and in the Global Analysis of Section 2.2. We give also the number of degrees of freedom (n.d.f.), and the corresponding goodness of fit (g.o.f.) assuming for X^2_{min} a χ^2 distribution with n.d.f. degrees of freedom.

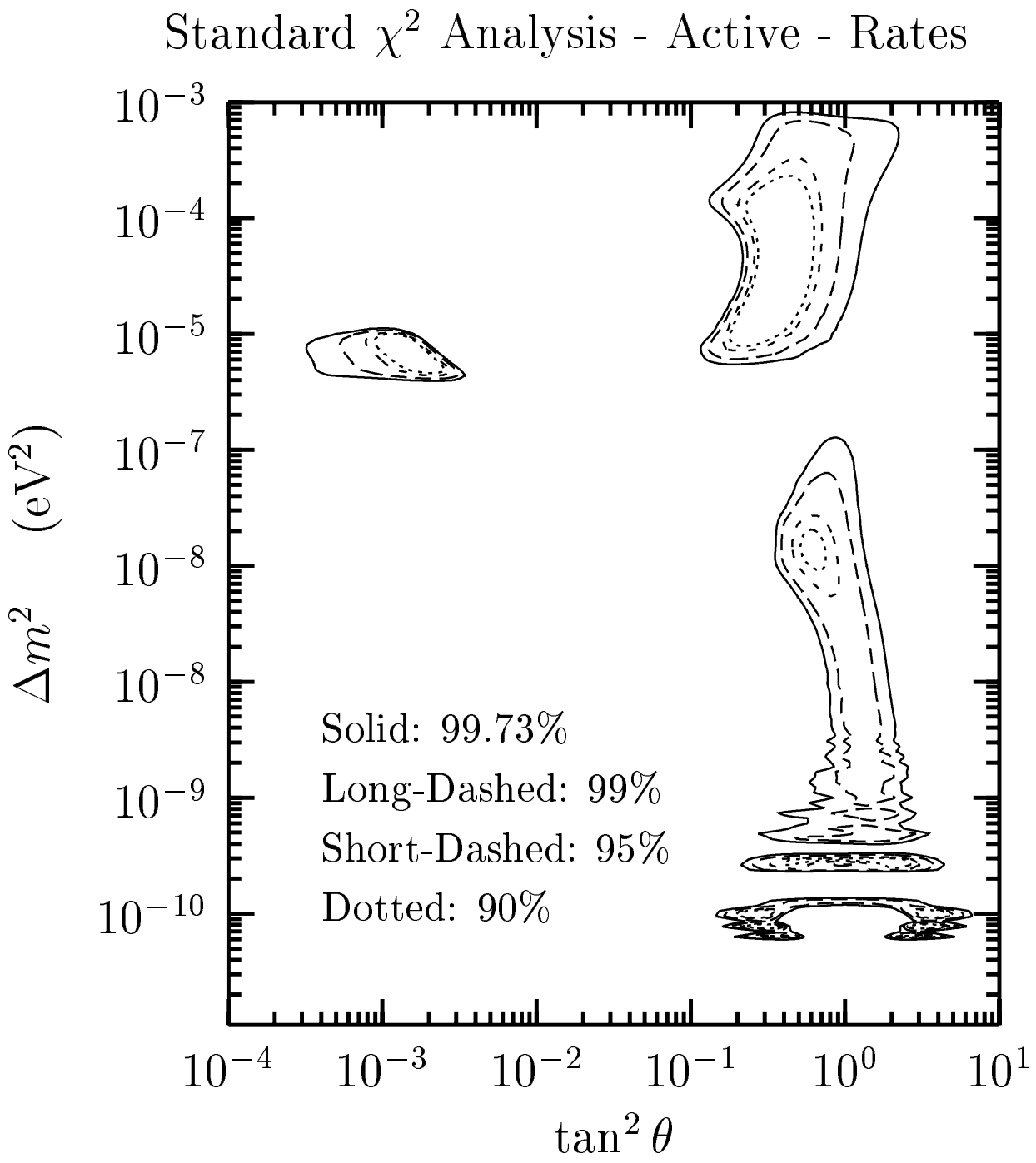

Figure 1: Allowed regions in the standard least-squares Rates Analysis (Section 2.1) of solar neutrino rates and CHOOZ data in terms of $\nu_e \to \nu_a$ transitions.

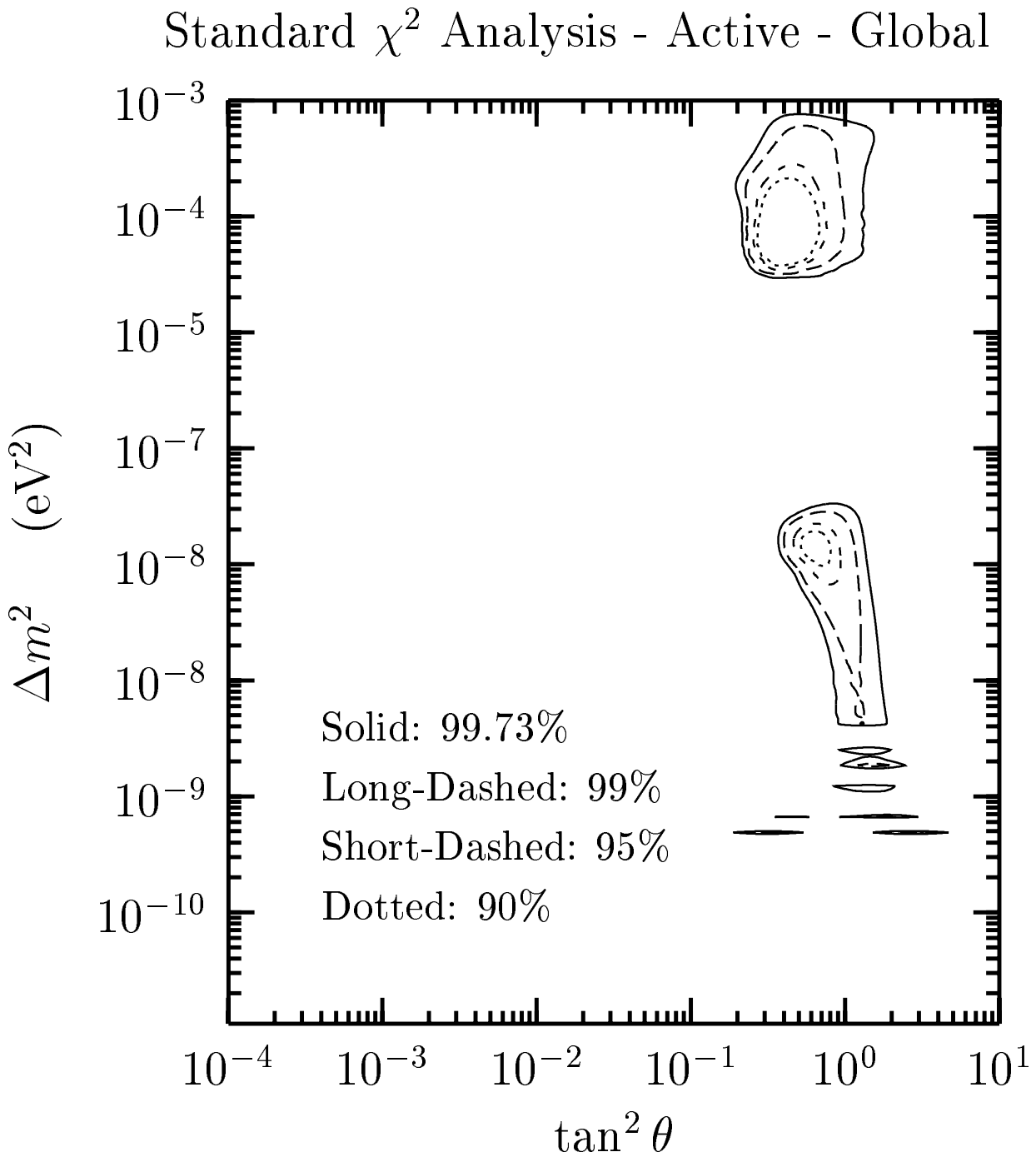

Figure 2: Allowed regions in the standard least-squares Global Analysis (Section 2.2) of the rates of the Homestake, GALLEX+GNO+SAGE and SNO experiments, the Super-Kamiokande day and night electron energy spectra and CHOOZ data in terms of $\nu_e \to \nu_a$ transitions.

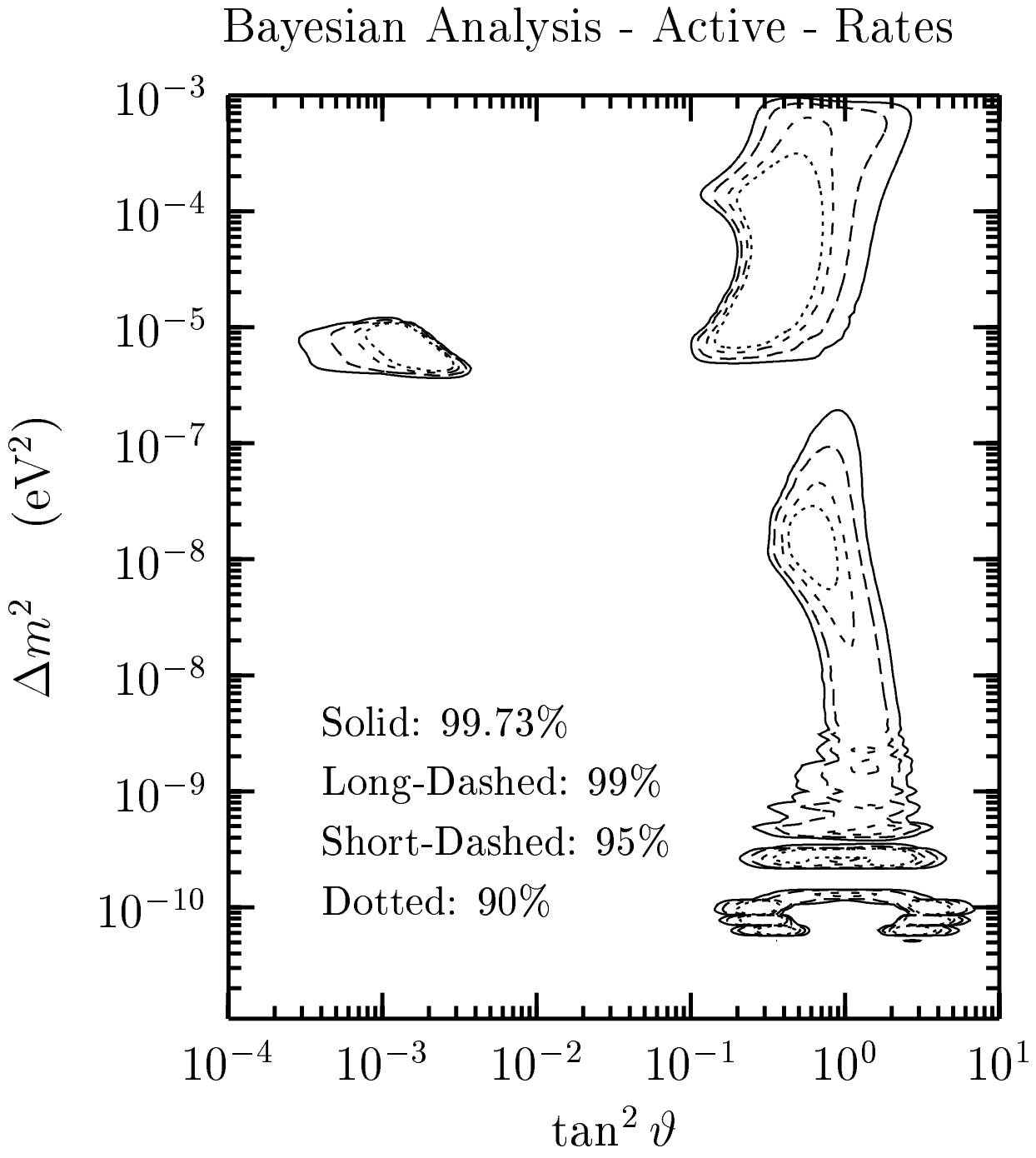

Figure 3: Credible regions obtained with the Bayesian Rates Analysis of solar neutrino rates and CHOOZ data in terms of $\nu_e \to \nu_a$ transitions. The dotted, short-dashed, long-dashed and solid curves enclose credible regions with, respectively, 90%, 95%, 99% and 99.73% posterior probability to contain the true values of $\tan^2\vartheta$ and Δm^2.

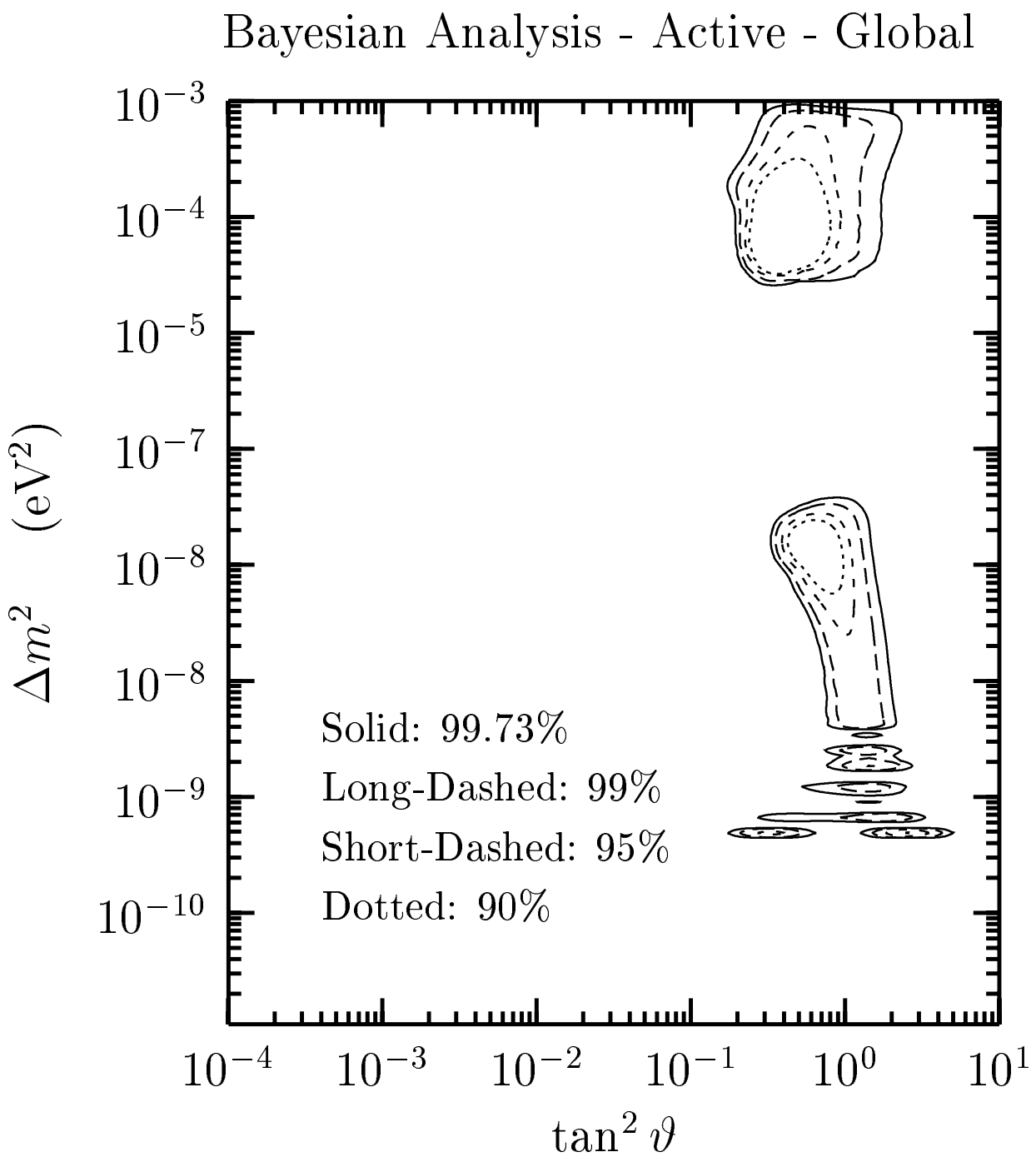

Figure 4: Credible regions obtained with the Bayesian Global Analysis of the rates of the Homestake, GALLEX+GNO+SAGE and SNO experiments, the Super-Kamiokande day and night electron energy spectra and CHOOZ data in terms of $\nu_e \to \nu_a$ transitions. The dotted, short-dashed, long-dashed and solid curves enclose credible regions with, respectively, 90%, 95%, 99% and 99.73% posterior probability to contain the true values of $\tan^2\vartheta$ and Δm^2.

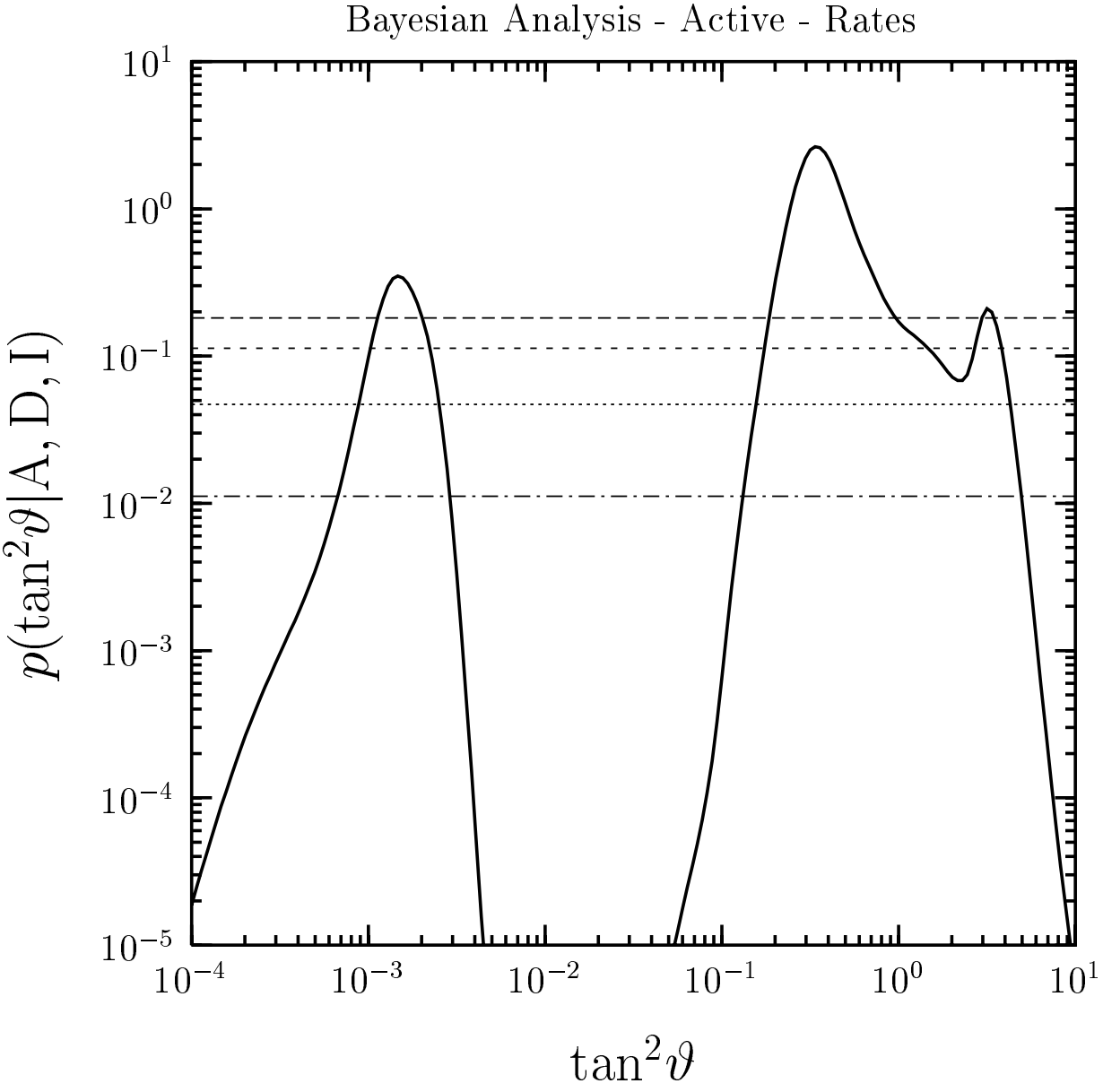

Figure 5: Marginal posterior probability distribution for $\tan^2\vartheta$ obtained with the Bayesian Rates Analysis of solar neutrino rates and CHOOZ data in terms of $\nu_e \to \nu_a$ transitions (solid curve). The intervals in which the solid curve lies above the long-dashed, short-dashed, dotted, and dash-dotted lines have, respectively, 90%, 95%, 99% and 99.73% posterior probability to contain the true value of $\tan^2\vartheta$.

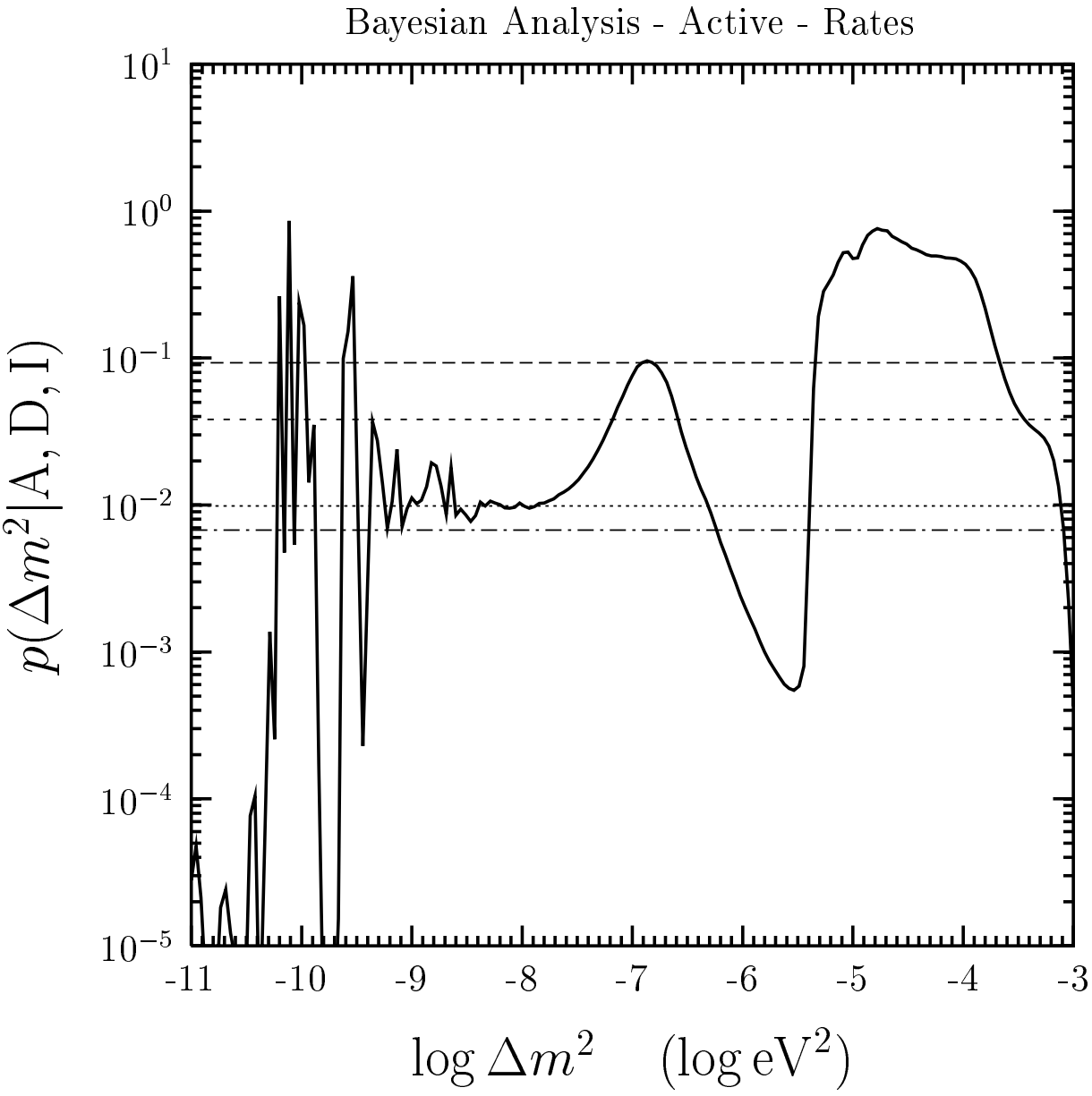

Figure 6: Marginal posterior probability distribution for Δm^2 obtained with the Bayesian Rates Analysis of solar neutrino rates and CHOOZ data in terms of $\nu_e \to \nu_a$ transitions (solid curve). The intervals in which the solid curve lies above the long-dashed, short-dashed, dotted, and dash-dotted lines have, respectively, 90%, 95%, 99% and 99.73% posterior probability to contain the true value of Δm^2.

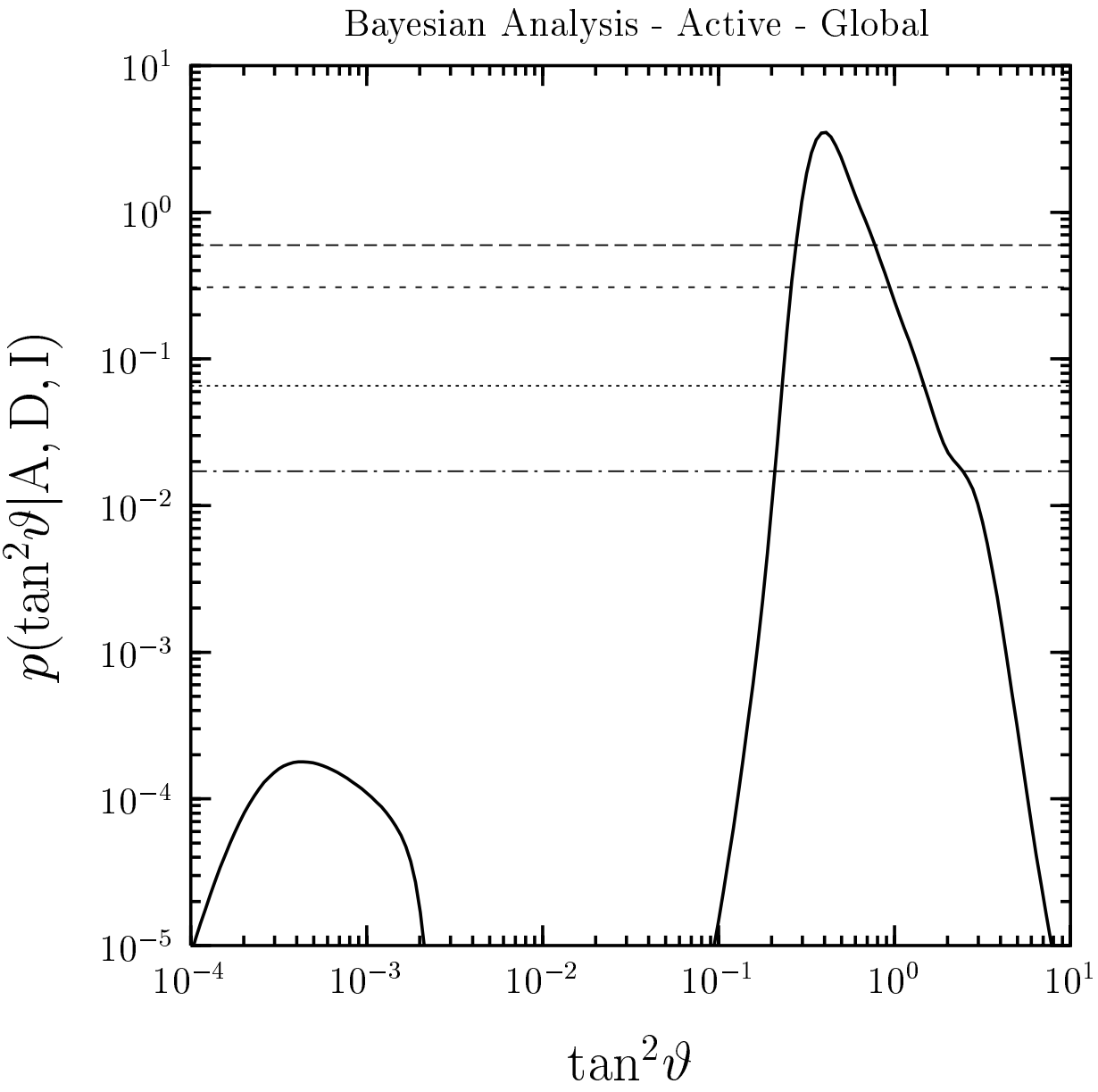

Figure 7: Marginal posterior probability distribution for $\tan^2\vartheta$ obtained with the Bayesian Global Analysis of the rates of the Homestake, GALLEX+GNO+SAGE and SNO experiments, the Super-Kamiokande day and night electron energy spectra and CHOOZ data in terms of $\nu_e \to \nu_a$ transitions (solid curve). The intervals in which the solid curve lies above the long-dashed, short-dashed, dotted, and dash-dotted lines have, respectively, 90%, 95%, 99% and 99.73% posterior probability to contain the true value of $\tan^2\vartheta$.

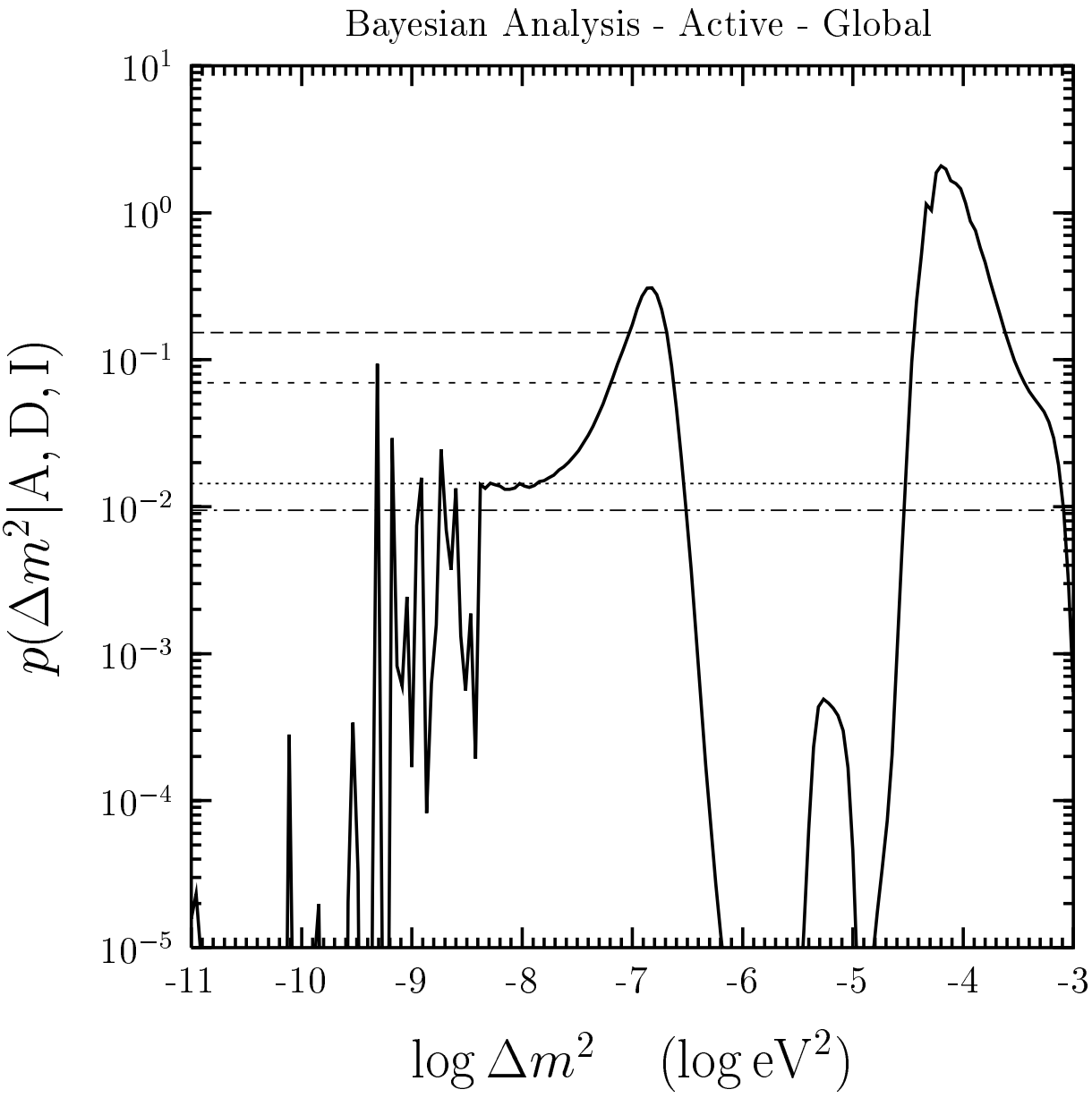

Figure 8: Marginal posterior probability distribution for Δm^2 obtained with the Bayesian Global Analysis of the rates rates of the Homestake, GALLEX+GNO+SAGE and SNO experiments, the Super-Kamiokande day and night electron energy spectra and CHOOZ data in terms of $\nu_e \to \nu_a$ transitions (solid curve). The intervals in which the solid curve lies above the long-dashed, short-dashed, dotted, and dash-dotted lines have, respectively, 90%, 95%, 99% and 99.73% posterior probability to contain the true value of Δm^2.